

1/18/65

PERSONAL COPY

UNCLASSIFIED

~~CONFIDENTIAL~~

NASA TECHNICAL  
MEMORANDUM



NASA TM X-1051

NASA TM X-1051

CLASSIFICATION CHANGED

FOR REFERENCE

UNCLASSIFIED

By authority of

STAR Date 12/31/70  
U.S. No 24 Blm  
LIBRARY COPY 3-11-

JAN 10 1965

LANGLEY RESEARCH CENTER  
LIBRARY, NASA  
LANGLEY STATION  
HAMPTON, VIRGINIA

AERODYNAMIC SEPARATION  
CHARACTERISTICS OF CONCEPTUAL  
PARALLEL-STAGED REUSABLE  
LAUNCH VEHICLE AT MACH 3 TO 6

*by John P. Decker and P. Kenneth Pierpont*  
*Langley Research Center*  
*Langley Station, Hampton, Va.*

NATIONAL AERONAUTICS AND SPACE ADMINISTRATION • WASHINGTON, D. C. • JANUARY 1965

UNCLASSIFIED

~~CONFIDENTIAL~~

UNCLASSIFIED  
~~CONFIDENTIAL~~

CLASSIFICATION CHANGED

To UNCLASSIFIED

By authority of ESTAR Date 2/3/76

U-8 No. 24

Blm  
3-11-71

AERODYNAMIC SEPARATION CHARACTERISTICS OF  
CONCEPTUAL PARALLEL-STAGED REUSABLE  
LAUNCH VEHICLE AT MACH 3 TO 6

By John P. Decker and P. Kenneth Pierpont

Langley Research Center  
Langley Station, Hampton, Va.

GROUP 4  
Downgraded at 3 year intervals;  
declassified after 12 years

CLASSIFIED DOCUMENT—TITLE UNCLASSIFIED

This material contains information affecting the national defense of the United States within the meaning of the espionage laws, Title 18, U.S.C., Secs. 793 and 794, the transmission or revelation of which in any manner to an unauthorized person is prohibited by law.

NOTICE

This document should not be returned after it has satisfied your requirements. It may be disposed of in accordance with your local security regulations or the appropriate provisions of the Industrial Security Manual for Safe-Guarding Classified Information.

NATIONAL AERONAUTICS AND SPACE ADMINISTRATION

UNCLASSIFIED  
~~CONFIDENTIAL~~

UNCLASSIFIED

~~CONFIDENTIAL~~

AERODYNAMIC SEPARATION CHARACTERISTICS OF  
CONCEPTUAL PARALLEL-STAGED REUSABLE  
LAUNCH VEHICLE AT MACH 3 TO 6\*

By John P. Decker and P. Kenneth Pierpont  
Langley Research Center

SUMMARY

A wind-tunnel investigation was made of an approximate 1/125-scale model of a horizontal-take-off horizontal-landing reusable launch vehicle. The model consisted of a winged reusable first stage, a winged reusable second stage, and a third-stage winged reusable spacecraft with an expendable maneuvering propulsion package. The two upper stages or combinations thereof were arranged in tandem, and this combination was placed parallel to the first-stage reusable booster. The upper-stage configurations were separated in parallel from the first stage. The wind-tunnel tests were conducted at Mach numbers of 3.00, 4.50, and 6.00, at angles of attack from approximately  $-4^\circ$  to  $12^\circ$ , and for spacing distances based upon the equivalent base diameter of the first-stage fuselage of 0.25 to 1.65. The Reynolds number per foot varied from  $1.0 \times 10^6$  to  $2.1 \times 10^6$ .

The results show that large changes in both lift coefficient and pitching-moment coefficient occurred for both stages and were dependent on the configuration, Mach number, and spacing. The magnitude of the changes in pitching-moment coefficient and lift coefficient would present a stability and control problem for both the first stage and the upper stages during separation, especially if separation occurred at high dynamic pressures.

INTRODUCTION

The separation of two major components of an orbital launch vehicle has up to the present been largely limited to vehicles whose stages were arranged in tandem as in a staged colinear missile. For this class of vehicles, the integrity of only the upper stage is involved at stage separation. However, for many concepts of future generation launch vehicles, the integrity of both stages may be required whether the stages are arranged in parallel or in tandem. Because of the interest in parallel-arranged stages especially for completely reusable as well as for expendable launched vehicle systems, the Langley

---

\*Title, Unclassified.

~~CONFIDENTIAL~~  
UNCLASSIFIED

~~UNCLASSIFIED~~

Research Center has initiated an investigation to examine the aerodynamic problems associated with the separation of parallel-arranged stages.

The purpose of the present paper is to present experimental aerodynamic results at stage separation of a representative complete reusable launch vehicle system at supersonic and hypersonic speeds. For a vehicle of this type, the integrity of both the first and upper stages becomes a requirement so that each may complete its representative portion of the mission and effect a safe return to earth for reuse. Although the aerodynamic characteristics during separation at design staging conditions may be highly important, the ability to perform a safe separation during or following a malfunction leading to an abort maneuver may be equally important. No differentiation between what may be considered staging conditions or abort conditions will be made; instead, the results will be employed to discern some of the effects of the physical phenomena on the aerodynamic characteristics of the two major components of the vehicle selected for this investigation.

The selected launch vehicle consisted of a conceptual design of a horizontal-take-off and horizontal-landing system for which each stage was a wing-body configuration intended to fly back and land horizontally. The launch vehicle was similar to the vehicle for which aerodynamic characteristics were reported in references 1 and 2. Consideration has been limited to the conditions in which both major components would remain essentially parallel during the early phase of the separation maneuver. The employment of a parallelogram or trapeze mechanism is one method to achieve this type of separation. Other modes of separation such as variable incidence and/or longitudinal displacement have not been considered herein, in order to reduce the number of variables for the present investigation.

Tests were conducted on a 1/125-scale model of the launch vehicle (ref. 1) in a 2-foot hypersonic facility at the Langley Research Center at nominal Mach numbers of 3.00, 4.50, and 6.00, and at angles of attack from approximately  $-4^\circ$  to  $12^\circ$ . The two major components (first-stage and upper-stage configuration) were individually mounted to measure forces and moments for spacing distances based upon the equivalent base diameter of the first-stage fuselage of 0.25 to 1.65. The Reynolds number per foot varied from approximately  $1.0 \times 10^6$  to  $2.1 \times 10^6$ .

#### SYMBOLS

The aerodynamic characteristics of the first stage and the upper stages have been referred to the stability axes. The moment reference center for both the first stage and the upper stages was 7.48 inches forward of the base in the stage separation plane. The aerodynamic coefficients for the first stage are based on the geometry of the first-stage wing whereas the aerodynamic coefficients for the upper-stage configurations are based on the geometry of the second-stage wing.

~~CONFIDENTIAL~~

UNCLASSIFIED

UNCLASSIFIED

~~CONFIDENTIAL~~

$C_L$	lift coefficient, $\frac{\text{Lift}}{qS}$
$C_D$	drag coefficient, $\frac{\text{Drag}}{qS}$
$C_m$	pitching-moment coefficient, $\frac{\text{Pitching moment}}{qS\bar{c}}$
$c$	local chord, ft
$\bar{c}$	reference mean aerodynamic chord based on total wing area, 0.733 ft for first-stage and 0.424 ft for upper-stage configurations
$d$	equivalent base diameter of first-stage fuselage, 0.192 ft
$h$	spacing between flat upper surface of first stage and flat lower surface of second stage (see fig. 1(b))
$M$	free-stream Mach number
$P_t$	stagnation pressure, atm
$q$	free-stream dynamic pressure, lb/sq ft
$S$	reference wing area, 0.440 sq ft for first-stage and 0.188 sq ft for upper-stage configurations
$T_t$	stagnation temperature, $^{\circ}R$
$x_{cp}$	location of center of pressure forward of base of first-stage reusable booster or upper-stage configuration
$\alpha$	angle of attack (referred to stage-separation plane), deg
$h/d$	nondimensional spacing, based upon equivalent base diameter of first-stage fuselage
$\frac{x_{cp}}{d}$	nondimensional location of center of pressure, based upon equivalent base diameter of first-stage fuselage
$C_D, \alpha, C_L, \alpha, C_m, \alpha$	drag, lift, and pitching-moment coefficients at an angle of attack
$\Delta C_D$	incremental change in drag coefficient at $\alpha = 0^{\circ}$ , $(C_D, \alpha=0)_{h/d} - (C_D, \alpha=0)_{h/d=\infty}$
$\Delta C_L$	incremental change in lift coefficient at $\alpha = 0^{\circ}$ , $(C_L, \alpha=0)_{h/d} - (C_L, \alpha=0)_{h/d=\infty}$

~~CONFIDENTIAL~~

UNCLASSIFIED

~~UNCLASSIFIED~~  
~~CONFIDENTIAL~~

$\Delta C_m$  incremental change in pitching-moment coefficient at  $\alpha = 0^\circ$ ,  
 $(C_m, \alpha=0)_{h/d} - (C_m, \alpha=0)_{h/d=\infty}$

$\frac{\Delta x_{cp}}{d}$  incremental change in center of pressure,  $\left(\frac{x_{cp}}{d}\right)_{h/d} - \left(\frac{x_{cp}}{d}\right)_{h/d=\infty}$

Subscripts:

I first-stage reusable booster

II upper-stage configurations

Component designations:

B second-stage fuselage

W second-stage wing

F second-stage vertical fins

M maneuver propulsion package

S spacecraft

S' forebody fairing

#### DESCRIPTION OF MODEL

The complete launch vehicle, which was identical to that of reference 1, and its components are shown in figure 1. The launch vehicle consisted of a first and second stage which were both winged and reusable, and a third-stage winged reusable spacecraft with an expendable space-maneuvering propulsion package. The two upper stages were arranged in tandem, and this combination was placed parallel to the first stage. Figure 1(b) shows the relative positions of the first stage and the upper stages for the present investigation. Principal model dimensions are presented in table I, and photographs of the first stage separated from various upper-stage configurations are shown in figure 2.

#### First-Stage Reusable Booster

The first-stage reusable booster consisted of a semicylindrical fuselage with an ogival forebody, a delta canard, and a delta wing with trapezoidal vertical fins mounted outboard on nacelles. (See fig. 1(c).) The wing had  $70^\circ$  leading-edge sweep and was a symmetrical wedge to the 40-percent-chord station with a constant 0.050c maximum thickness rearward to the 0.85c station. A wedge or boattail on the lower surface of the wing extended from 0.85c to the

~~CONFIDENTIAL~~  
UNCLASSIFIED

# UNCLASSIFIED

~~CONFIDENTIAL~~

wing trailing edge. (See fig. 1(d).) The wing was flat on the upper surface rearward of the 40-percent station to allow mating with the second-stage wing. The wing was set at an incidence angle of  $0^\circ$ . The requirement for a flat upper surface resulted in a wing dihedral angle of about  $3\frac{1}{2}^\circ$ . The exposed area of the canard was approximately 7 percent of the total first-stage wing area, and the distance between 0.25c of the canard and 0.25c of the first-stage wing was 1.4c of the wing.

The vertical fins were located outboard at two-thirds of the wing semi-span. The total fin area, which was equally distributed above and below the wing, was approximately 15 percent of the total wing area. The vertical fins had a panel aspect ratio of 1.15 and a taper ratio of 0.5. The nacelles were cylindrical with a parabolic nose and were considered to house the flyback engines. The nacelles formed the juncture between the first-stage wing and the vertical fins.

## Second-Stage Reusable Booster

The second-stage reusable booster consisted of a cylindrical fuselage and a trapezoidal wing with two outboard-mounted vertical fins located at two-thirds of the wing semispan. The fuselage incorporated a side fairing which extended vertically from the center line of the second-stage fuselage to the upper surface of the first-stage fuselage. The wing thickness was chosen to achieve a total profile thickness of 0.065c (based on the chord of the first-stage wing) when the first- and second-stage wings were mated. The forward 0.40c of the upper surface of the upper-stage wing formed a coplanar surface with the first-stage wing. A portion of the leading edge was removed to form a constant leading-edge radius on the second-stage wing identical to that of the first-stage wing. The purpose of this arrangement was to reduce the interference of the mated wings during launch. The second-stage vertical fins were similar to the first-stage vertical fins, but only the upper element was employed.

## Orbital Stage

The spacecraft was a wing-body configuration with toed-in, wing-tip-mounted vertical fins. (See fig. 1(e).) The spacecraft wing was unsymmetrical with the camber adjacent to the spacecraft pad, and the span (including vertical fins) was approximately equal to the width of the first-stage fuselage. A pad was used to support the spacecraft on the launch vehicle, but for this investigation, the pad was removed. (See fig. 1(b).)

The maneuver propulsion package was an expendable rocket booster designed as a short cylinder with the same diameter as the second-stage fuselage and incorporating the same type of side fairing as the second-stage fuselage. When the model was tested without the maneuver propulsion package, the spacecraft was moved rearward to connect directly with the second-stage fuselage. This configuration was considered to meet a mission requirement not needing appreciable in-orbit maneuvering.

~~CONFIDENTIAL~~

UNCLASSIFIED

A forebody fairing was tested in place of the spacecraft and adapter fairing, for which case the configuration was considered to place a ballistic payload into orbit.

#### APPARATUS AND TESTS

The tests of the present investigation were conducted in a 2-foot hypersonic facility at the Langley Research Center, which is described in reference 3. The nominal test Mach numbers were 3.00, 4.50, and 6.00, angles of attack from  $-4^\circ$  to approximately  $12^\circ$ , and spacing distances based upon the equivalent base diameter of first-stage fuselage of 0.25 to 1.65. The Reynolds number per foot varied from approximately  $1.0 \times 10^6$  to  $2.1 \times 10^6$ . No shock reflection or boundary-layer interference from the tunnel walls was present for the range of variables in this investigation.

Separate sting supports were provided for the first stage and the upper stages. Relative movement between the first stage and the upper stages was provided in the vertical plane by the support system to which the stings were attached. The two stages remained essentially parallel, with bases aligned, throughout the angle-of-attack range while the spacing distance was varied. (See fig. 1(b).)

Static aerodynamic force and moment data were simultaneously obtained for the first stage and the upper stages by use of individual internal six-component strain-gage balances. No composite configurations, that is, with the first stage and the upper stages connected, were tested in the present investigation. These data are obtained in reference 1.

All data were obtained with the model smooth; and at the Reynolds numbers of these tests laminar flow is considered to exist. The average test conditions and typical Reynolds number variation during the launch trajectory of the complete vehicle are given in the following table:

Test conditions			Reynolds number (based on overall length of first stage) for -	
M	$P_t$ , atm	$T_t$ , $^\circ R$	Test	Launch trajectory
3.00	1.0	580	$4.2 \times 10^6$	$7.0 \times 10^6$
4.50	1.5	760	2.0	2.4
6.00	3.4	810	2.2	1.6

It is seen from this table that the Reynolds numbers for the launch trajectory are in reasonable agreement with the test Reynolds numbers.

~~CONFIDENTIAL~~

UNCLASSIFIED

# UNCLASSIFIED

~~CONFIDENTIAL~~

The individual vehicle angles of attack were corrected for balance and sting deflection under load. The drags of the first stage and upper stages were corrected to correspond to a base pressure equal to the free-stream static pressure on the fuselage and that portion of the wing base intercepted by the fuselage.

The deviation in angle of attack of the upper stages in relation to the first stage is seen in figure 3 to be small at all angles of attack for  $M = 4.50$  and  $6.00$ . At  $M = 3.00$  and angles of attack greater than  $6^\circ$  this deviation becomes progressively larger and approaches  $1^\circ$  at the highest test angles of about  $13^\circ$ . The deviation in angle of attack is caused by the difference in forces and moments on the balance-sting combination for the first stage and the upper stages.

The accuracies of the coefficients based on instrument calibration and repeatability are estimated to be within the following limits:

M . . . . .	$\pm 0.005$
$\alpha$ . . . . .	$\pm 0.1$
$h/d$ . . . . .	$\pm 0.05$

## First stage:

$C_D$ . . . . .	$\pm 0.001$
$C_L$ . . . . .	$\pm 0.002$
$C_m$ . . . . .	$\pm 0.001$

## Upper stages:

$C_D$ . . . . .	$\pm 0.001$
$C_L$ . . . . .	$\pm 0.002$
$C_m$ . . . . .	$\pm 0.002$

## PRESENTATION OF RESULTS

The longitudinal aerodynamic characteristics of the first stage in the presence of various upper-stage configurations and of the various upper-stage configurations in presence of the first stage are shown in figures 4 to 13, some of the results being summarized in figures 14 to 17. The various upper-stage configurations are identified with letter symbols for purposes of clarification. (See symbol list for component identification.)

Figure

Longitudinal aerodynamic characteristics of the first stage in presence of the following upper-stage configurations:

BWFMS . . . . .	4
BMS . . . . .	5
BWFS . . . . .	6
BS . . . . .	7
BWFMS' . . . . .	8

~~CONFIDENTIAL~~

UNCLASSIFIED

Figure

Longitudinal aerodynamic characteristics of the following upper-stage configurations in the presence of the first stage:

BWFMS . . . . .	9
BMS . . . . .	10
BWFS . . . . .	11
BS . . . . .	12
BWFMS' . . . . .	13

Variation with spacing distance of the incremental changes in lift, pitching moment, and drag coefficient at zero angle of attack for the first-stage and various upper-stage configurations . . . . . 14

Schlieren photographs of the first stage in presence of BWFS . . . . . 15

Variation with spacing distance of the incremental changes in center of pressure at an angle of attack of 6° for the first-stage and upper-stage configurations . . . . . 16

Variation of the center of pressure with angle of attack for the first-stage and upper-stage configurations . . . . . 17

DISCUSSION

The results of the force and moment measurements made during the present investigation have been divided, insofar as practicable, into two principal parts. These two parts consist of the aerodynamic characteristics of the first stage in the presence of the upper-stage configurations and the aerodynamic characteristics of the upper-stage configurations in the presence of the first stage. Because of the complexity of the aerodynamic phenomena resulting from the present design concept, the discussion is limited to the salient effects of the mutual interferences. Furthermore, since "safe and practicable" separation of the major components is considered of paramount interest in the applied sense, the principal focus is directed toward stability and control implications.

First-Stage Characteristics

The basic aerodynamic data of figures 4 to 8 show that the proximity of the several upper-stage configurations produced marked but differing changes in the basic longitudinal aerodynamic coefficients of the first stage. These changes have been compared with the interference-free aerodynamic characteristics, superimposed from reference 1, and it can be seen that the region of significant influence generally extends beyond the maximum values of test spacing  $h/d$ . The interference between major components resulted in large negative displacement of lift curves, but with the exception of small local changes, had little effect on lift-curve slope. These displacements are dependent on configuration, Mach number, and spacing and amount to equivalent

CONFIDENTIAL

UNCLASSIFIED

# UNCLASSIFIED

~~CONFIDENTIAL~~

angle-of-attack increments of about  $2^\circ$  to  $4^\circ$  throughout the test angle range. Interpreted in terms of angle increments, the changes indicated may not appear to be large; however, the problem of guidance and control during the critical period of physical separation can be expected to be severe since it is the time rate of change of  $\Delta C_L$  associated with the normal component of velocity which will establish the control system requirements. Since a nonpropelled or coasting period which will degrade the system performance may exist during stage separation, it is desirable to have a rapid separation, that is, high separation normal velocity, and hence a large value of  $dC_L/dh$  will be expected.

Figure 14(a) further illustrates the behavior of the zero angle-of-attack lift-coefficient increments, as a function of vehicle spacing, for three typical upper-stage configurations. The behavior of the curves for the two configurations, having identical spacecraft but with the second-stage wing on or off, are similar for a given Mach number. The changes with Mach number are also similar. In general, as the spacing increases from the initial vehicle unlatch value, for example,  $h/d = 0.25$ , the interference effect  $\Delta C_L$  for this vehicle combination reaches a maximum and then gradually tends to approach the interference-free value at sufficiently large spacings. This trend seems clear for the data obtained for the two higher Mach numbers but is not obvious at  $M = 3.00$ , probably because insufficiently large spacings were achieved.

The basic data (figs. 4 to 8) show that at  $M = 4.50$  and  $6.00$  the first-stage stability did not change significantly with spacing. At  $M = 3.00$ , for the separation distances of these tests, the presence of the upper stages resulted in destabilizing changes. The data indicate that the first-stage stability is dependent on both Mach number and upper-stage configuration. As was observed for  $\Delta C_L$ , the changes in  $\Delta C_m$  shown in figure 14(a) for the configurations with second-stage wing on or off were nearly the same. It can be seen that changes in  $\Delta C_m$  with spacing were very nearly in phase with the variation of  $\Delta C_L$  with spacing for any test Mach number for these configurations.

An explanation of the observed behavior of both  $\Delta C_L$  and  $\Delta C_m$  may be obtained by assuming that the first-order interference effects were caused by the spacecraft principal shock-wave impingement on the first stage, and that only secondary effects were then incurred by subsequent reflections. The affected area and its location is almost directly proportional to the spacing  $h/d$  and inversely proportional to the tangent of the effective shock-wave angle of the primary disturbance caused by the upper-stage configuration. For the present models, at low Mach numbers and moderate spacing or at high Mach numbers and small spacing, the upper-stage principal disturbance would lie almost entirely in front of the first-stage wing leading edge, and the only reflections would consist of those from the first-stage fuselage. When, however, some critical combination of Mach number and spacing occurred, the influence of the principal disturbance would be felt over most of the first-stage wing and thereby produce the maximum interference for both force and moments. For a given Mach number, exceeding the critical spacing would result in the initial impingement and associated reflections moving progressively rearward until finally a sufficient spacing is reached that it no longer would

~~CONFIDENTIAL~~

UNCLASSIFIED

UNCLASSIFIED  
~~CONFIDENTIAL~~

impinge on the first stage at all, that is, an interference-free condition. For a model producing as complex a flow field as the one used in the present investigation, it is difficult to support this argument quantitatively; however, qualitative verification can be obtained by examining schlieren photographs, typical examples of which are shown in figure 15. From the available evidence, therefore, it is concluded that the first-order effects of the upper-stage configuration on the first-stage vehicle are primarily functions of the strength of the principal disturbance, its effective source position, and Mach number.

Although the preceding discussion has been applicable at  $\alpha = 0^\circ$ , the basic data show similar effects over a wide angle-of-attack range. At angles of attack of  $6^\circ$ , for example, figure 16 shows the results plotted as the change in center of pressure with spacing. In this representation, the effects of normal-force and pitching-moment interference effects are combined. The critical spacing (maximum interference effect) has apparently been reached for  $M = 3.00$ , and it progressively decreases with increasing Mach number as anticipated from the foregoing discussion. Figure 17 illustrates further the configuration sensitivity of the center-of-pressure change with angle of attack. Although the type of vehicle employed in this investigation would fly nearly a ballistic flight path, it is doubtful whether angles of attack as large as those shown would be reached. Such large angles and their effects may be important, however, in the case of a malfunction requiring an abort separation.

#### Upper-Stage Characteristics

The basic aerodynamic data of figures 9 to 13 show that the proximity of the first stage to the several upper-stage configurations produced large but different changes in the basic longitudinal aerodynamic coefficients. The results have been compared with the interference-free aerodynamic characteristics superimposed on the figures. In contrast to the results shown earlier for the first stage, not only were there large displacements in both lift coefficient and pitching-moment coefficient for any given angle of attack, but also severe nonlinearities are shown.

The incremental changes in  $C_L$  and  $C_m$  at  $\alpha = 0^\circ$  plotted as functions of spacing  $h/d$  in figure 14(b) show that, in contrast to the increments shown previously for the first stage, the upper-stage increments are significantly changed when the second-stage wing is on or off. This change could be anticipated since, if it is the principal disturbance generated by the spacecraft which contributes the primary effects on the first stage, it is the reflection of this principal disturbance which would contribute the primary effects on the upper-stage configuration. Because this disturbance, upon reflection, would spread three-dimensionally, the upper-stage wing surfaces, in addition to the body, would be under its influence. The increment in lift coefficient is, of course, positive and opposite to the sign of the first-stage increment since the local pressure on the under surfaces of the upper stage has increased because of the disturbance. Two maximums in  $\Delta C_L$  (fig. 14(b)) of differing magnitude are apparent for the upper-stage configurations with the second-stage wing on. The first maximum follows the same trend as that for the first stage;

~~CONFIDENTIAL~~

UNCLASSIFIED

## UNCLASSIFIED

that is, some critical spacing occurs which decreases with increasing Mach number. The second maximum probably results from the disturbance created by the first-stage wing acting on the second-stage wing. Only the data at the highest test Mach number ( $M = 6.00$ ) indicate clearly the existence of this second maximum in  $\Delta C_L$ ; the  $M = 4.50$  results suggest that the second maximum exists since the curves are diverging from the abscissa; and at  $M = 3.00$ , it may be inferred that a similar trend would have been shown if sufficient spacing distances had been achieved. The observed changes in  $\Delta C_m$  seem to support the same argument. In any event, for the configurations tested, the effects of the interference during separation are shown to be both large in magnitude and to vary rapidly with spacing.

At angles of attack other than  $0^\circ$ , for example, in the range of about  $\pm 4^\circ$ , it is believed that the primary influence on the lift-curve slope arises from the orderly change in the compression or expansion of the field about the first-stage forebody. At higher positive angles, the data suggest some form of progressive blanketing, which is shown by the decrease in lift-curve slope to near zero. This condition is best illustrated at the smaller  $h/d$  values in figures 9 to 13.

The combined effects of normal-force and pitching-moment increments have been shown in figure 16 by presenting the change in upper-stage center of pressure with spacing for the three test Mach numbers at  $\alpha = 6^\circ$ . Changes as large as 3.00 diameters are shown. Both large positive and negative shifts occurred, which are nearly the same magnitude for this particular angle of attack, for either the wing-on or wing-off configurations. At  $M = 6.00$  it appears that for the largest spacing tested  $h/d = 1.65$ , nearly interference-free center-of-pressure conditions have been achieved. At  $M = 4.50$ , extrapolation suggests that  $h/d = 2.5$  would have to be reached before interference-free conditions would be achieved. In contrast, the results shown at  $M = 3.00$  suggest that interference-free conditions may have been reached, but on the basis that the trends shown for both the first-stage configuration as well as the upper-stage configuration are valid, another significant change may be expected before the curves would again approach interference-free conditions. It appears to be

purely coincidental that  $\left( \frac{\Delta x_{cp}}{d} \right)_{II}$  has reached a value near zero for the maxi-

mum test value of  $h/d$ . In any event the shifts in center of pressure with spacing are large. Figure 17 shows the variation of the center-of-pressure increment with angle of attack and serves to illustrate, as discussed previously, the seriousness of off-design separation conditions.

### CONCLUDING REMARKS

An investigation has been conducted in a 2-foot hypersonic facility at the Langley Research Center to ascertain some of the aerodynamic characteristics during separation of a staged parallel mounted reusable launch vehicle. Various upper-stage configurations were separated in parallel from the first stage. The wind-tunnel tests were conducted at Mach numbers of 3.00, 4.50, and 6.00, at

~~CONFIDENTIAL~~

UNCLASSIFIED

~~CONFIDENTIAL~~

angles of attack from approximately  $-4^{\circ}$  to  $12^{\circ}$ , and for spacing distances based on the equivalent base diameter of the first-stage fuselage of 0.25 to 1.65. The Reynolds number per foot varied from  $1.0 \times 10^6$  to  $2.1 \times 10^6$ .

For the first-stage configuration, stage separation over the Mach number range of these tests produced generally insignificant changes in either the lift-curve slopes or the longitudinal stability, except at a Mach number of 3.00, where close proximity of the upper-stage configurations resulted in destabilizing changes. The first-stage stability and lift characteristics were found to be dependent on both Mach number and upper-stage configuration. Large increments in both lift coefficient as well as pitching-moment coefficient, which were relatively constant throughout the angle-of-attack range, coupled with large rates of change of the increments with spacing, were attributed to separation interference.

For the upper-stage configurations, stage separation incurred large changes and produced nonlinearities in both lift-curve slope and longitudinal stability. Extremely large increments in both lift coefficient and pitching-moment coefficient, as well as large rates of change with spacing, were attributed to separation interference.

The observed changes in forces and moments, at small angles of attack, are believed to have been primarily caused for the first stage by impingement on the first stage of the principal upper-stage disturbance, and for the upper-stage configuration by the first-disturbance reflection. At high positive angles for the upper-stage configurations, the data suggest some form of progressive blanketing since the lift-curve slope decreases to near zero. Generally, the interference increments measured were dependent on configuration, Mach number, and spacing.

The present results indicate that potentially hazardous stability and control problems can be expected at hypersonic speeds for either stage or abort separation conditions, especially if the separation occurs at high dynamic pressures. In addition, the guidance and control requirements for either the first stage or upper stage will change significantly if more than a single upper-stage configuration is considered for use on the same first stage. The conclusion should not be inferred, at this time, that separation of parallel-arranged stages at significant dynamic pressures is impracticable, since the present investigation has examined only one method of separation, that is, each vehicle remained essentially parallel and in the same longitudinal position with respect to the other vehicle at all times. Assessment of the feasibility of separating parallel-arranged stages will require in addition to measured static aerodynamic coefficients inclusion of both dynamic and elastic effects of both major components of the vehicle.

Langley Research Center,  
National Aeronautics and Space Administration,  
Langley Station, Hampton, Va., October 9, 1964.

UNCLASSIFIED

UNCLASSIFIED

~~CONFIDENTIAL~~

REFERENCES

1. Clark, Larry R.; and Decker, John P.: Longitudinal Aerodynamic Characteristics of a Model of a Horizontal-Take-Off Reusable Launch Vehicle at Mach Numbers From 3 to 6. NASA TM X-1030, 1964.
2. Clark, Larry R.; and Pierpont, P. Kenneth: Transonic Characteristics of a Hydrogen-Fueled Multistage Horizontal-Take-Off Reusable Launch Vehicle. NASA TM X-1008, 1964.
3. Stokes, George M.: Description of a 2-Foot Hypersonic Facility at the Langley Research Center. NASA TN D-939, 1961.

~~CONFIDENTIAL~~

UNCLASSIFIED

UNCLASSIFIED

TABLE I.- GEOMETRIC DESIGN CHARACTERISTICS OF MODEL

## First stage:

## Fuselage:

Length, in. . . . .	23.760
Equivalent base diameter, in. . . . .	2.304
Maximum height, in. . . . .	1.922
Nose radius, in. . . . .	0.096
Base area, sq in. . . . .	4.164

## Wing:

Total area, sq in. . . . .	63.360
Exposed area, sq in. . . . .	34.432
Span, in. . . . .	9.600
Root chord, in. . . . .	13.200
Tip chord, in. . . . .	0
Maximum thickness, percent chord . . . . .	5.00
Leading-edge sweep angle, deg . . . . .	70
Leading-edge radius, in. . . . .	0.024
Mean aerodynamic chord, in. . . . .	8.800
Moment reference center, percent mean aerodynamic chord . . . . .	15
Moment reference center, in. from base . . . . .	7.480

## Vertical fins:

Area (exposed), sq in. . . . .	2.304
Height (exposed), in. . . . .	1.152
Root chord, in. . . . .	2.664
Tip chord, in. . . . .	1.332
Leading-edge sweep angle, deg . . . . .	60
Trailing-edge sweep angle, deg . . . . .	29.921
Leading-edge radius, in. . . . .	0.024

## Wing nacelles:

Length, in. . . . .	3.982
Maximum diameter, in. . . . .	0.576
Fineness ratio . . . . .	6.910
Nose radius, in. . . . .	0.096

## Canard:

Total area, sq in. . . . .	12.804
Exposed area, sq in. . . . .	4.478
Span, in. . . . .	4.320
Root chord, in. . . . .	5.928
Tip chord, in. . . . .	0
Maximum thickness, percent chord . . . . .	5
Leading-edge sweep angle, deg . . . . .	70
Leading-edge radius, in. . . . .	0.024

## Second stage:

## Fuselage:

Length, in. . . . .	9.600
Equivalent base diameter, in. . . . .	1.368
Base area, sq in. . . . .	1.464

CONFIDENTIAL

UNCLASSIFIED

## UNCLASSIFIED

~~CONFIDENTIAL~~

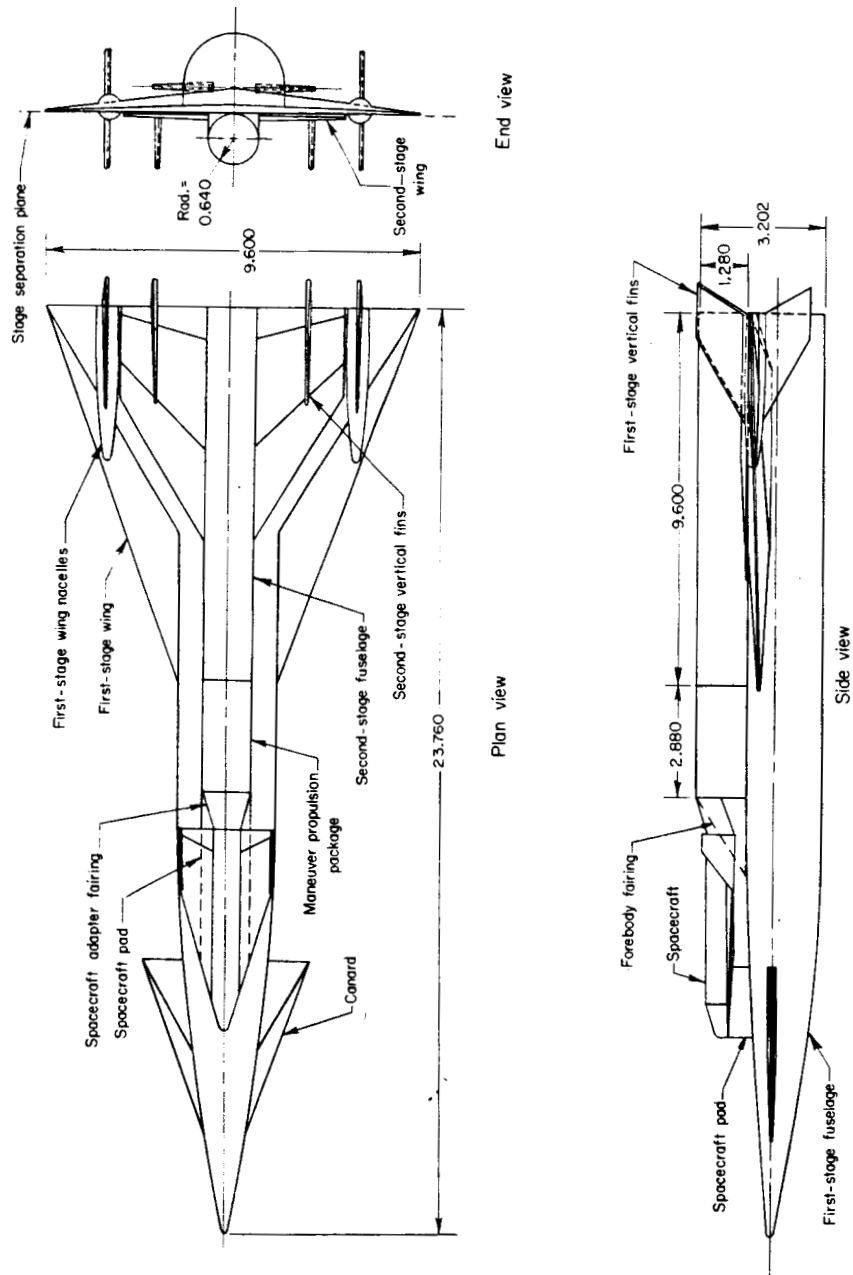
TABLE I.- GEOMETRIC DESIGN CHARACTERISTICS OF MODEL - Concluded

Wing:	
Total area, sq in. . . . .	27.072
Exposed area, sq in. . . . .	18.612
Span, in. . . . .	5.760
Root chord, in. . . . .	7.068
Tip chord, in. . . . .	2.311
Maximum thickness, percent chord . . . . .	2.800
Leading-edge sweep angle, deg . . . . .	58.753
Leading-edge radius, in. . . . .	0.024
Mean aerodynamic chord, in. . . . .	5.085
Moment reference center, in. from base . . . . .	7.480
Vertical fins:	
Area (exposed), sq in. . . . .	2.276
Height, in. . . . .	1.249
Root chord, in. . . . .	2.580
Tip chord, in. . . . .	1.332
Leading-edge sweep angle, deg . . . . .	60
Trailing-edge sweep angle, deg . . . . .	29.921
Leading-edge radius, in. . . . .	0.024
Maneuver propulsion package:	
Length, in. . . . .	2.880
Equivalent circular diameter, in. . . . .	1.368
Spacecraft:	
Fuselage:	
Length, including interstage, in. . . . .	6.048
Diameter, in. . . . .	0.672
Interstage base diameter, in. . . . .	1.280
Interstage taper, included angle, deg . . . . .	35.200
Length of nose cone, in. . . . .	0.857
Nose-cone included angle, deg . . . . .	35
Nose radius, in. . . . .	0.096
Wing:	
Total area, sq in. . . . .	8.527
Exposed area, sq in. . . . .	5.347
Span, in. . . . .	2.506
Root chord, in. . . . .	5.296
Tip chord, in. . . . .	1.589
Maximum thickness, percent chord . . . . .	5
Leading-edge sweep angle, deg . . . . .	72.500
Leading-edge radius, in. . . . .	0.024
Wing nose radius, in. . . . .	0.096
Vertical fins:	
Area, sq in. . . . .	0.866
Height, in. . . . .	0.858
Root chord, in. . . . .	1.589
Tip chord, in. . . . .	0.480
Maximum thickness, percent chord . . . . .	5
Leading-edge sweep angle, deg . . . . .	55
Leading-edge radius, in. . . . .	0.024
Lateral inclination angle, deg . . . . .	3

~~CONFIDENTIAL~~

UNCLASSIFIED

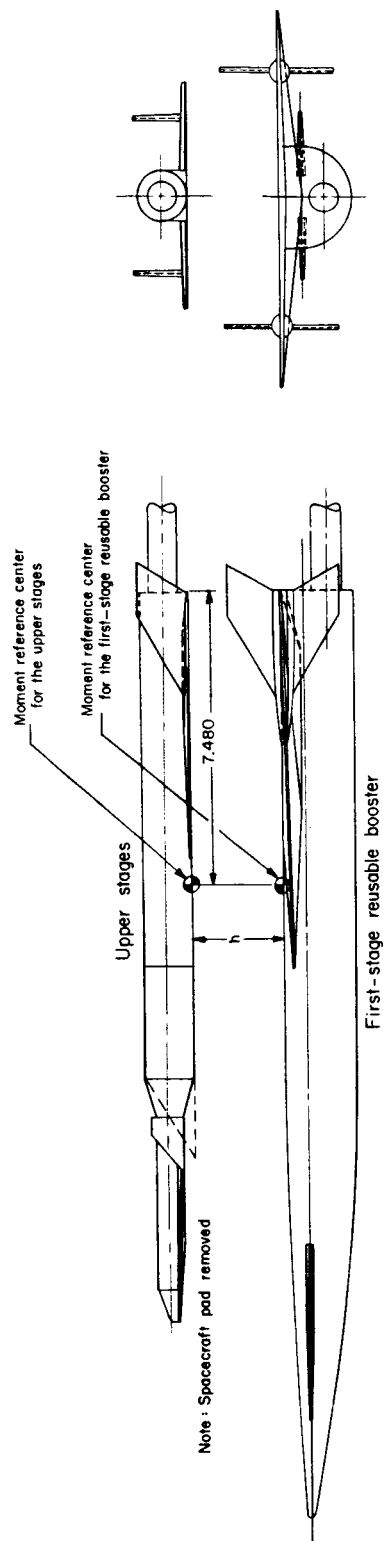
UNCLASSIFIED  
CONFIDENTIAL



(a) General arrangement of the launch vehicle prior to separation.

Figure 1.- Arrangement and geometric details of a three-stage horizontal-take-off reusable booster system.  
All linear design dimensions are in inches.

UNCLASSIFIED  
~~CONFIDENTIAL~~



(b) General arrangement of the first-stage reusable booster and the upper stages during stage separation investigation.

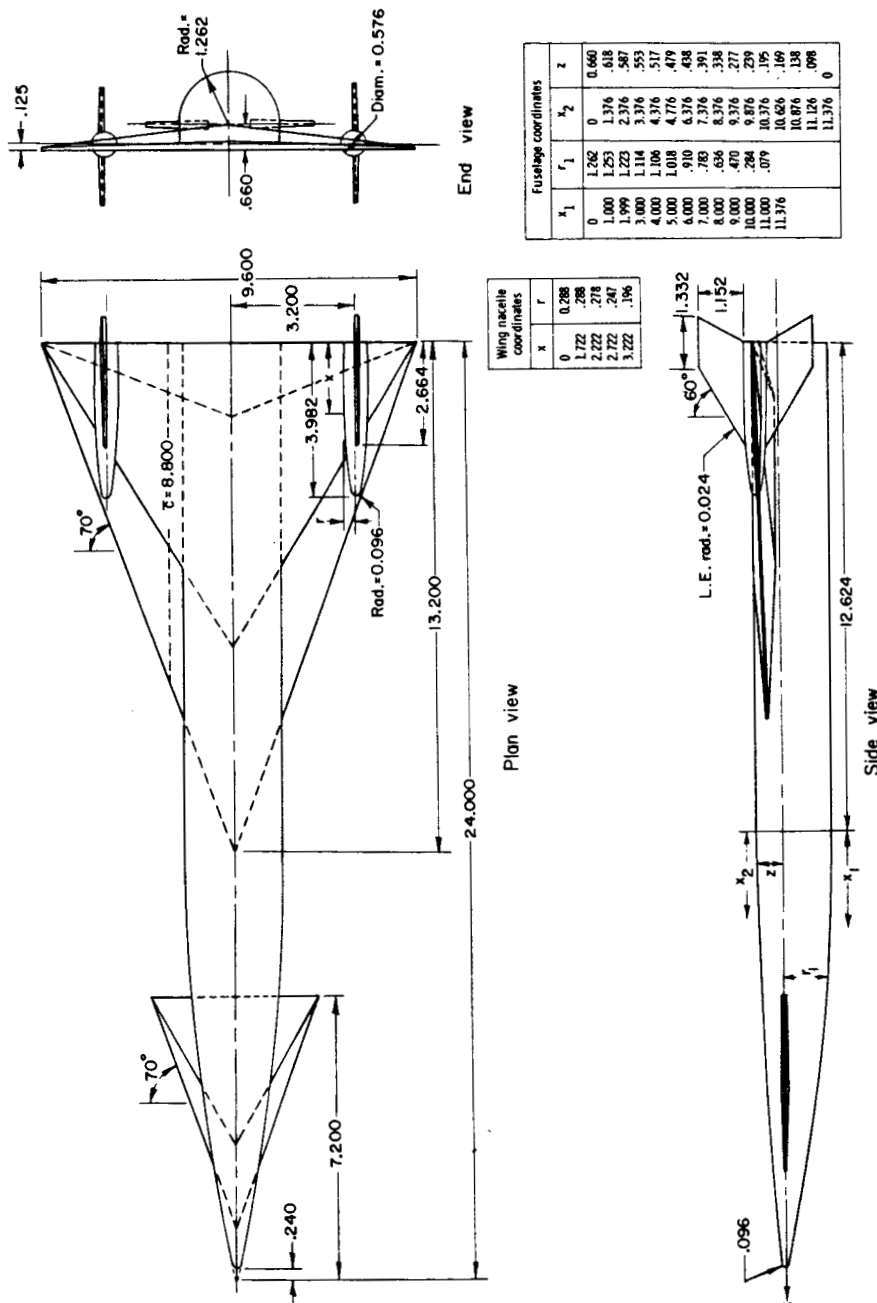
Figure 1.- Continued.

~~CONFIDENTIAL~~

UNCLASSIFIED

UNCLASSIFIED

~~CONFIDENTIAL~~



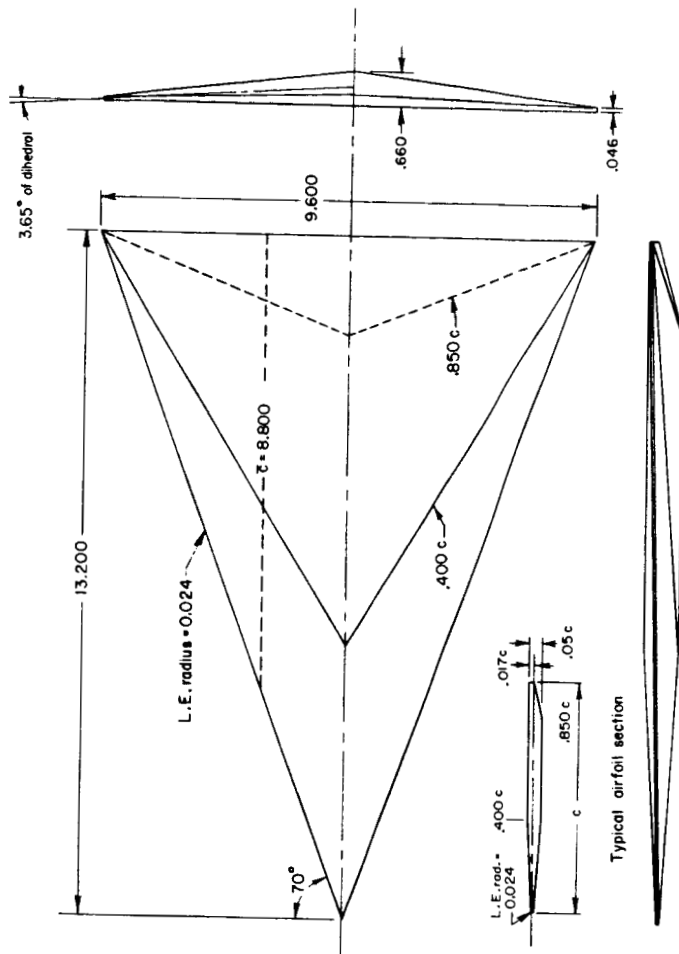
(c) First-stage reusable booster.

Figure 1.- Continued.

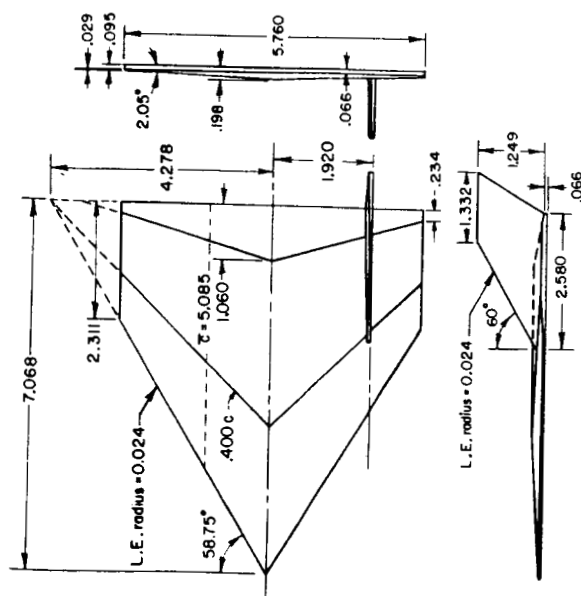
~~CONFIDENTIAL~~

UNCLASSIFIED

UNCLASSIFIED



First-stage wing



Second-stage wing

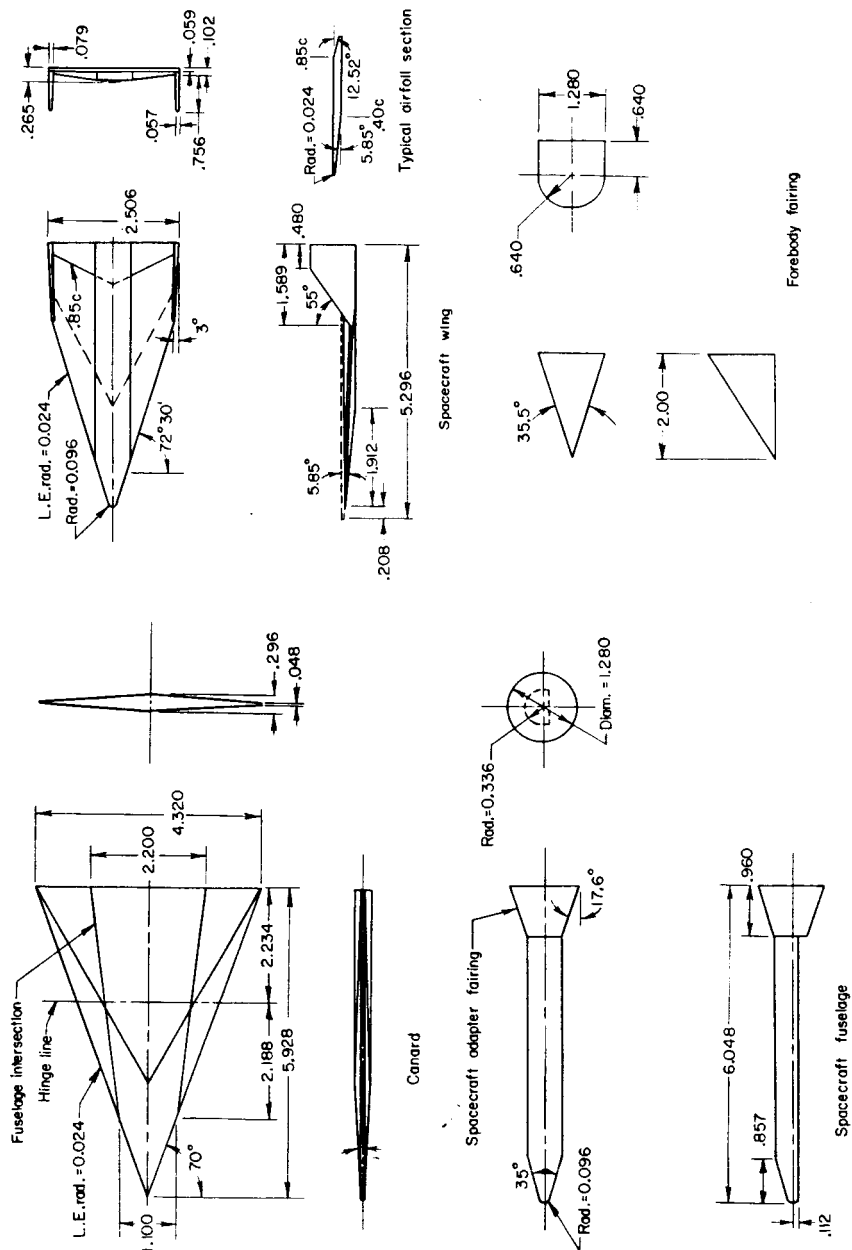
(d) Details of component parts.

Figure 1.- Continued.

UNCLASSIFIED

UNCLASSIFIED

CONFIDENTIAL



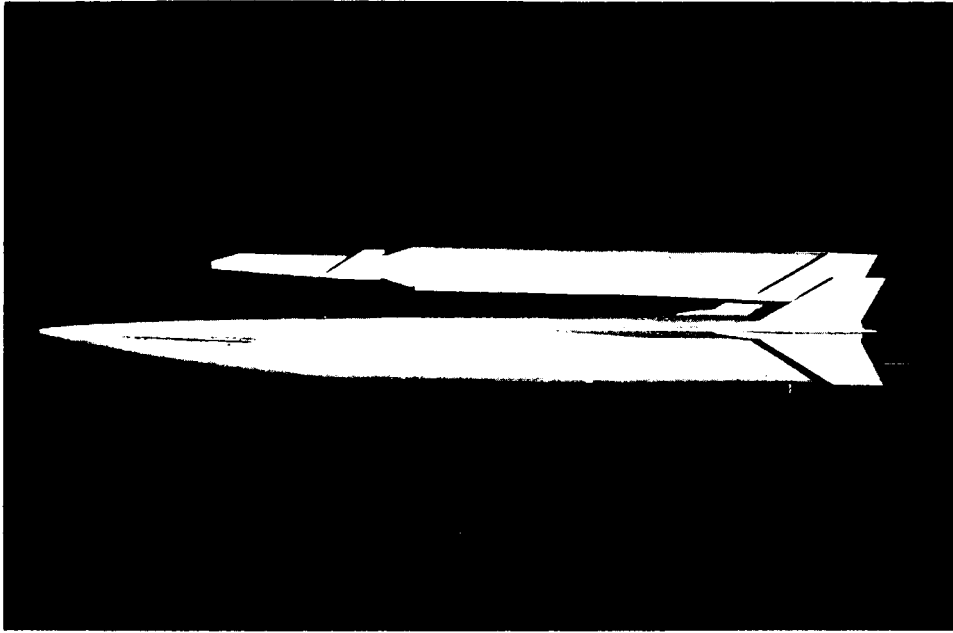
(e) Details of component parts.

Figure 1.- Concluded.

CONFIDENTIAL

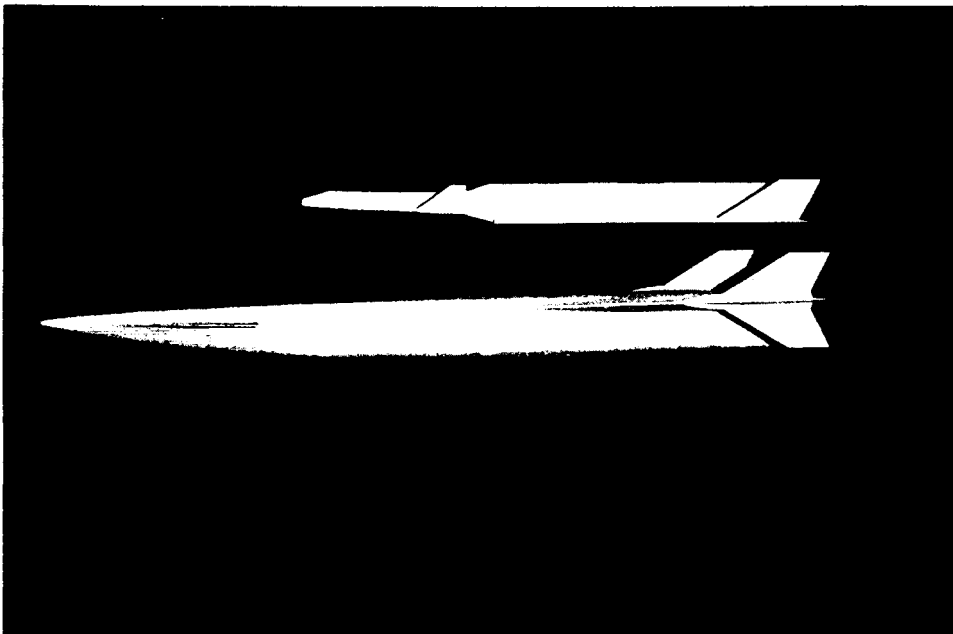
UNCLASSIFIED

UNCLASSIFIED  
~~CONFIDENTIAL~~



(a) Complete upper stages;  $h/d = 0.25$ .

L-64-3209



(b) Complete upper stages without the maneuver propulsion package;  $h/d = 1.00$ .

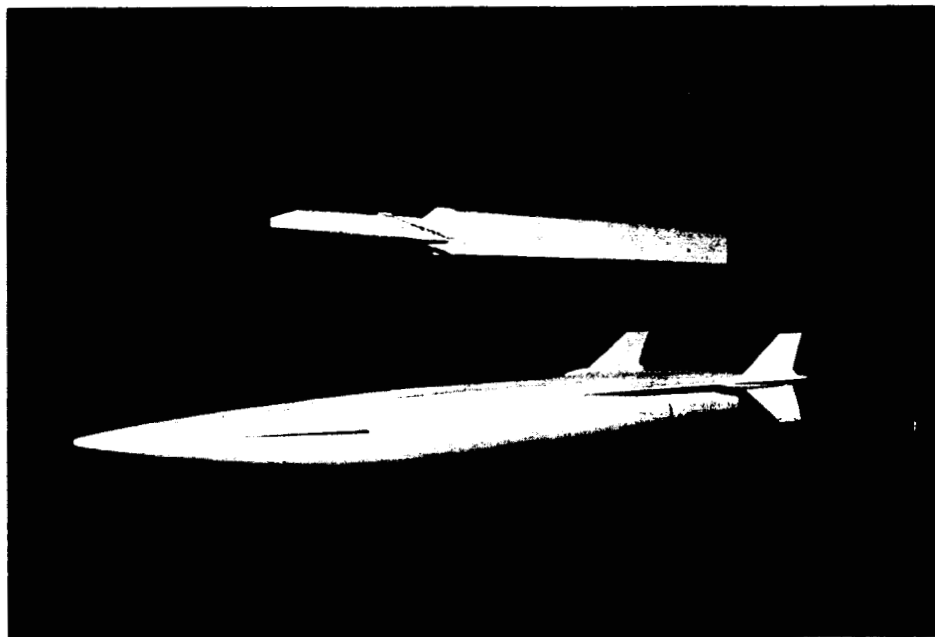
L-64-3219

Figure 2.- Photographs of various upper-stage configurations separated from the first-stage reusable booster.

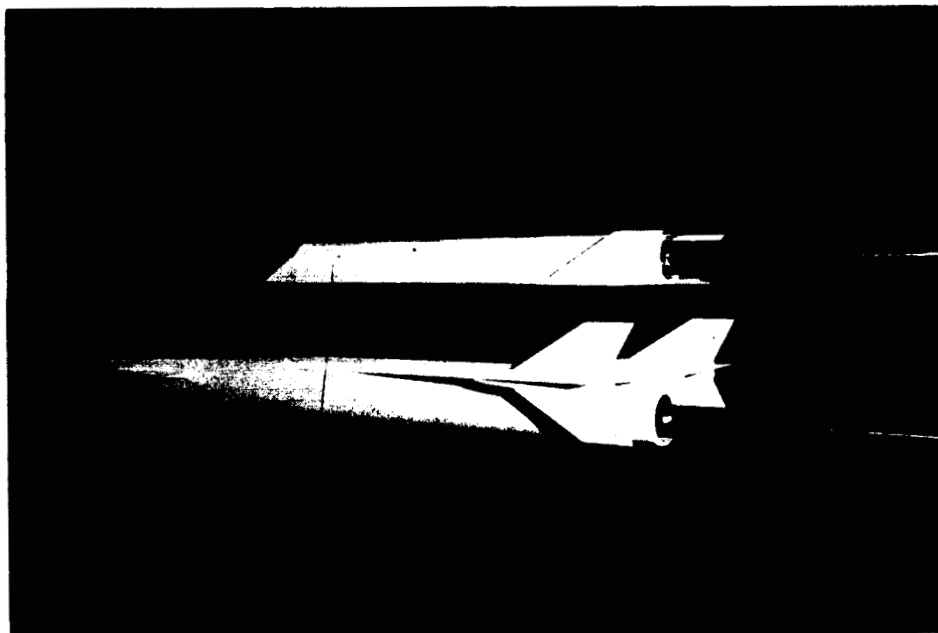
~~CONFIDENTIAL~~

UNCLASSIFIED

UNCLASSIFIED



(c) Complete upper stages without the second-stage wing;  $h/d = 1.50$ . I-64-3225



(d) Complete upper stages with the spacecraft and adapter fairing replaced with a forebody fairing;  $h/d = 1.00$ . I-64-3211

Figure 2.- Concluded.

UNCLASSIFIED

UNCLASSIFIED

UNCLASSIFIED

~~CONFIDENTIAL~~

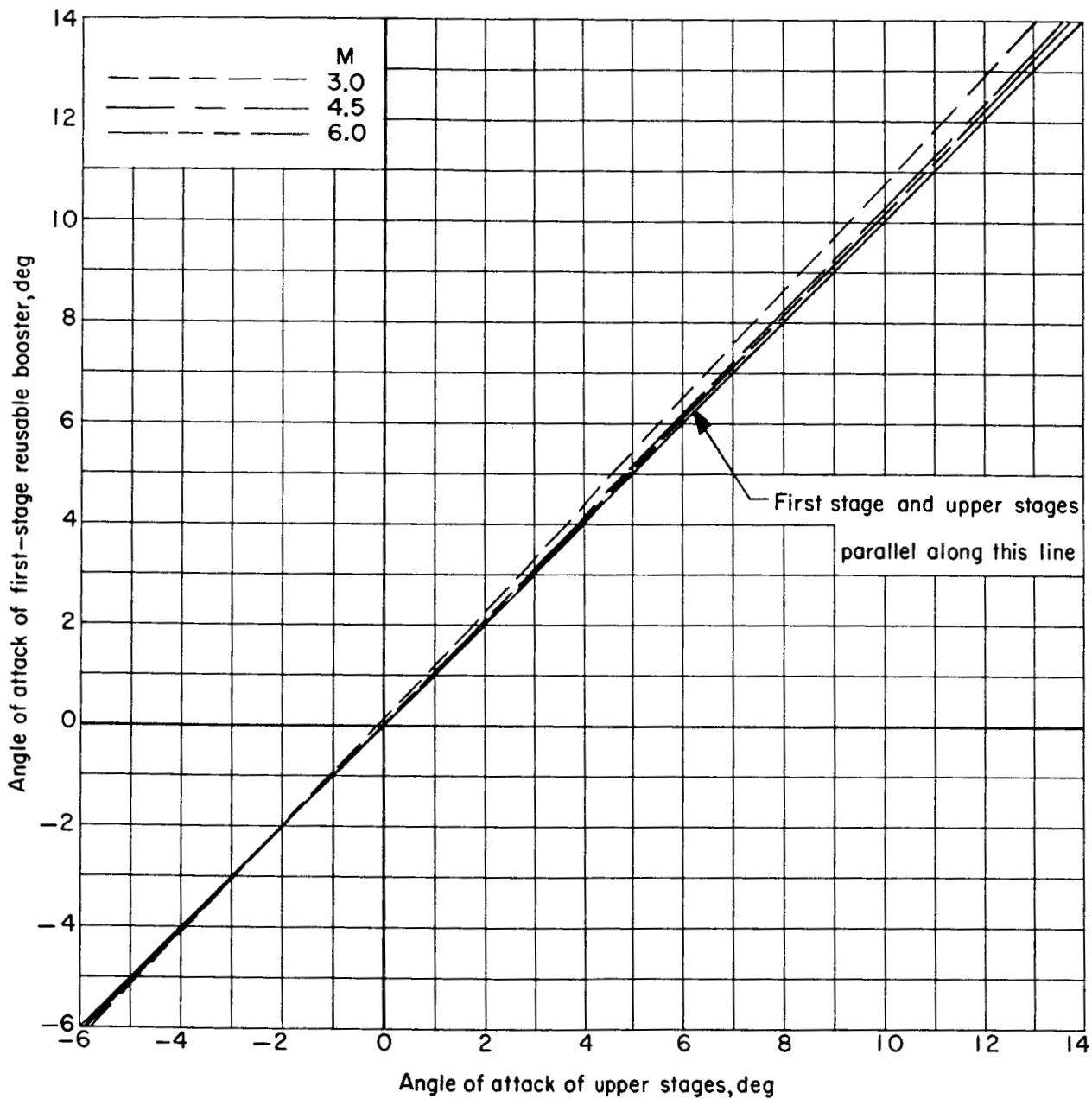
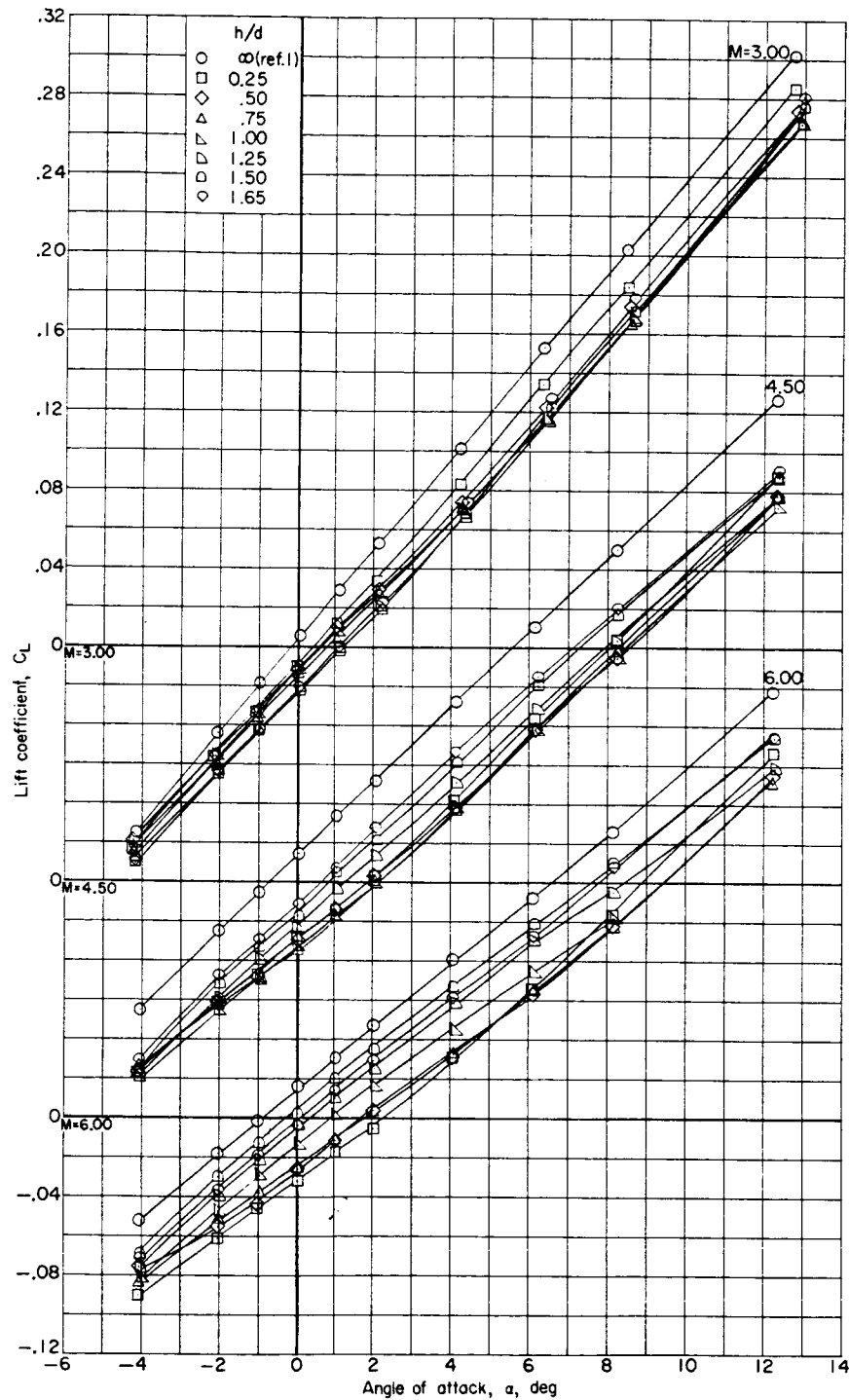


Figure 3.- Typical angle-of-attack deviation due to balance and sting deflection under load between the first-stage reusable booster and the upper stages.

~~CONFIDENTIAL~~

UNCLASSIFIED

UNCLASSIFIED

~~CONFIDENTIAL~~

(a) Variation of lift coefficient with angle of attack.

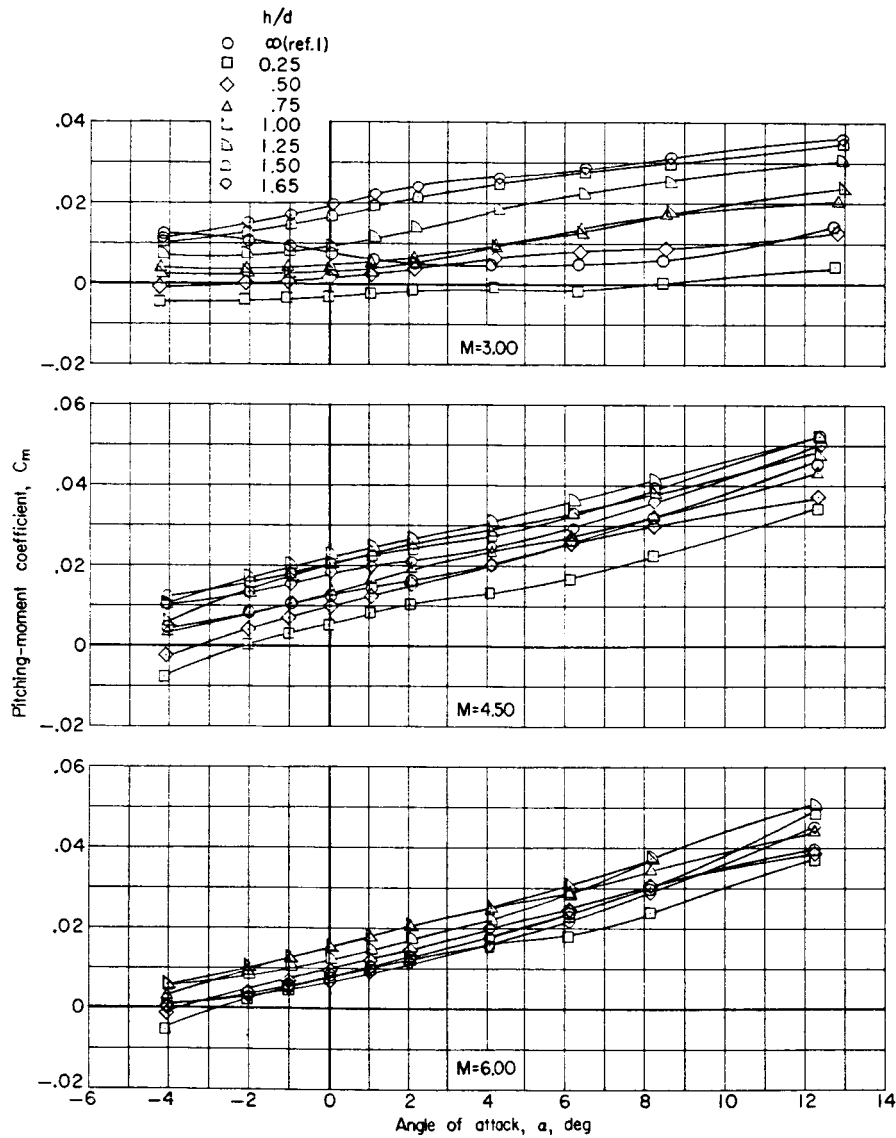
Figure 4.- Longitudinal aerodynamic characteristics of the first-stage reusable booster in presence of BWFS.

~~CONFIDENTIAL~~

UNCLASSIFIED

UNCLASSIFIED

~~CONFIDENTIAL~~



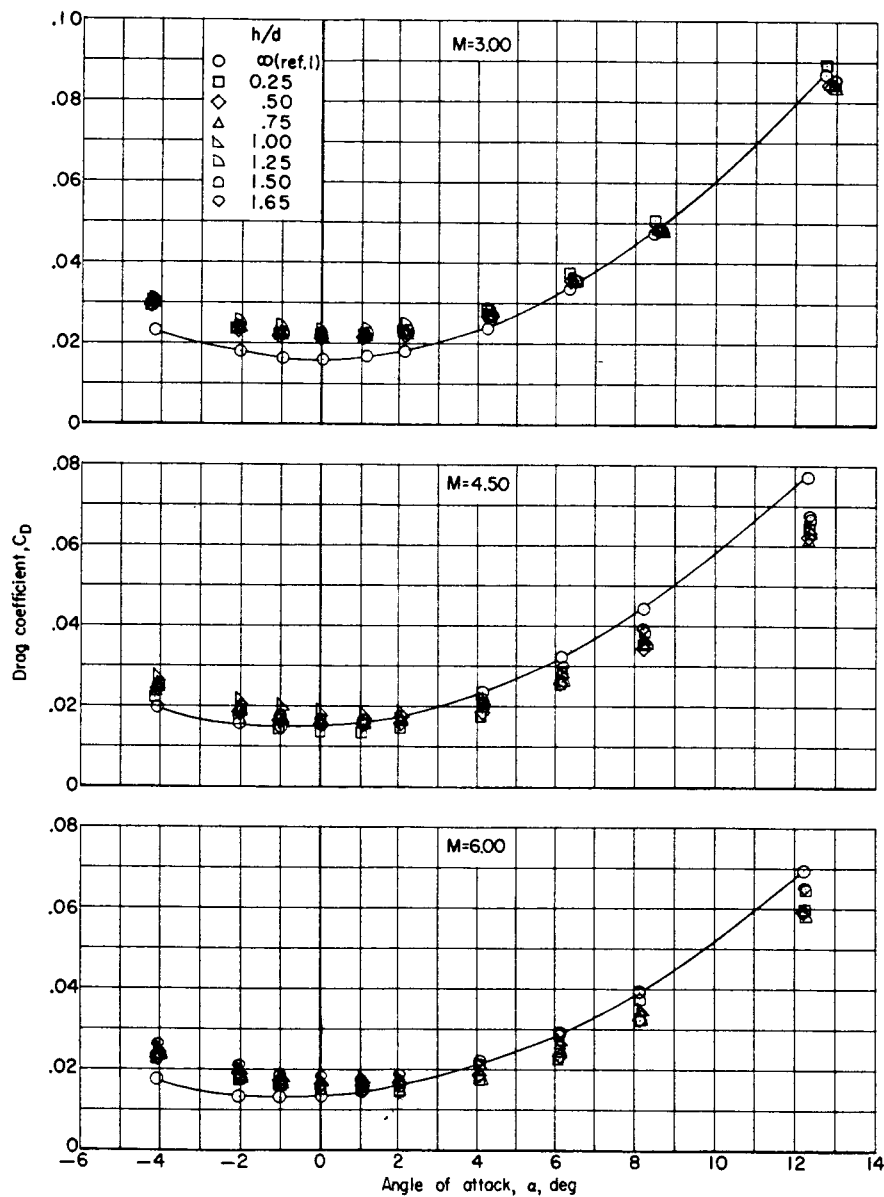
(b) Variation of pitching-moment coefficient with angle of attack.

Figure 4.- Continued.

~~CONFIDENTIAL~~

UNCLASSIFIED

UNCLASSIFIED  
~~CONFIDENTIAL~~



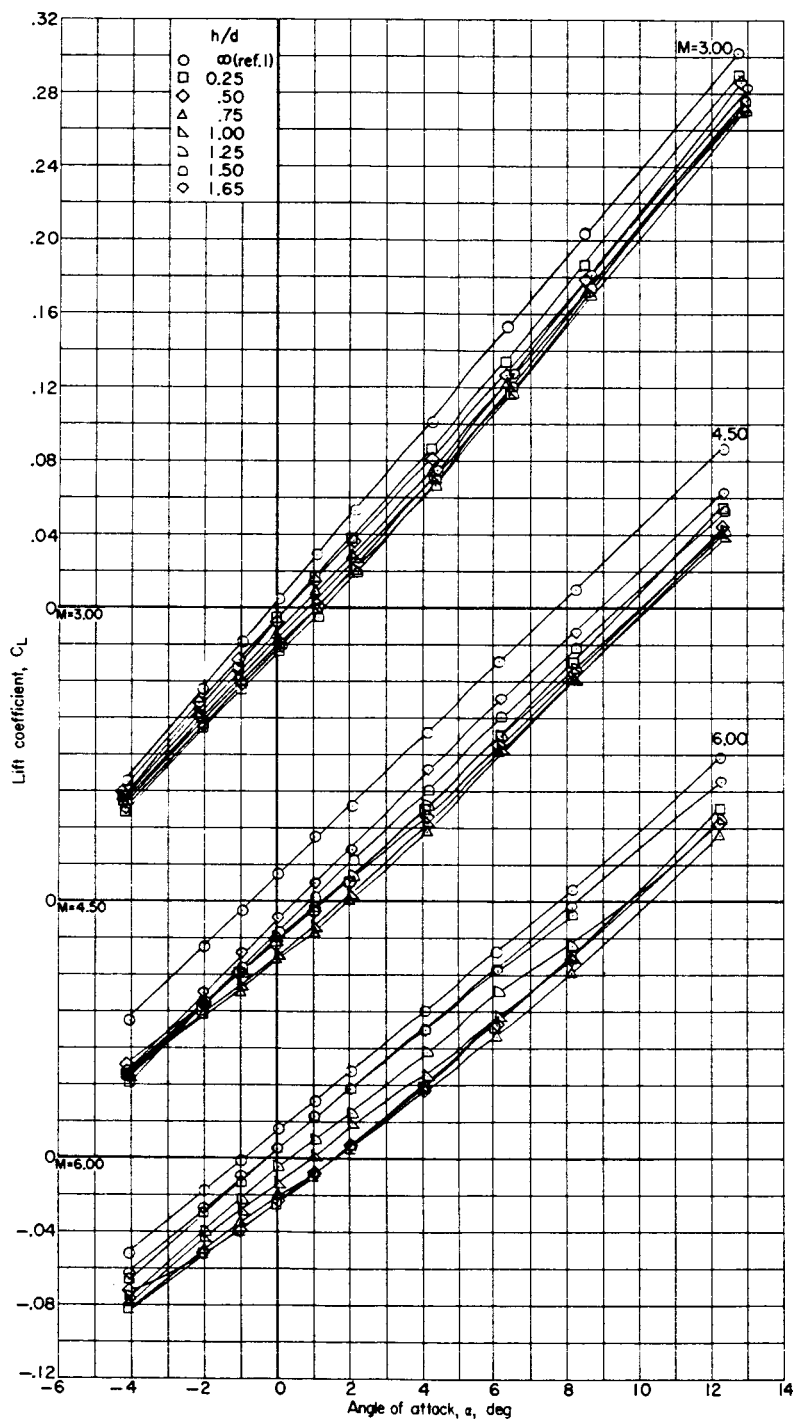
(c) Variation of drag coefficient with angle of attack.

Figure 4.- Concluded.

~~CONFIDENTIAL~~

UNCLASSIFIED

UNCLASSIFIED

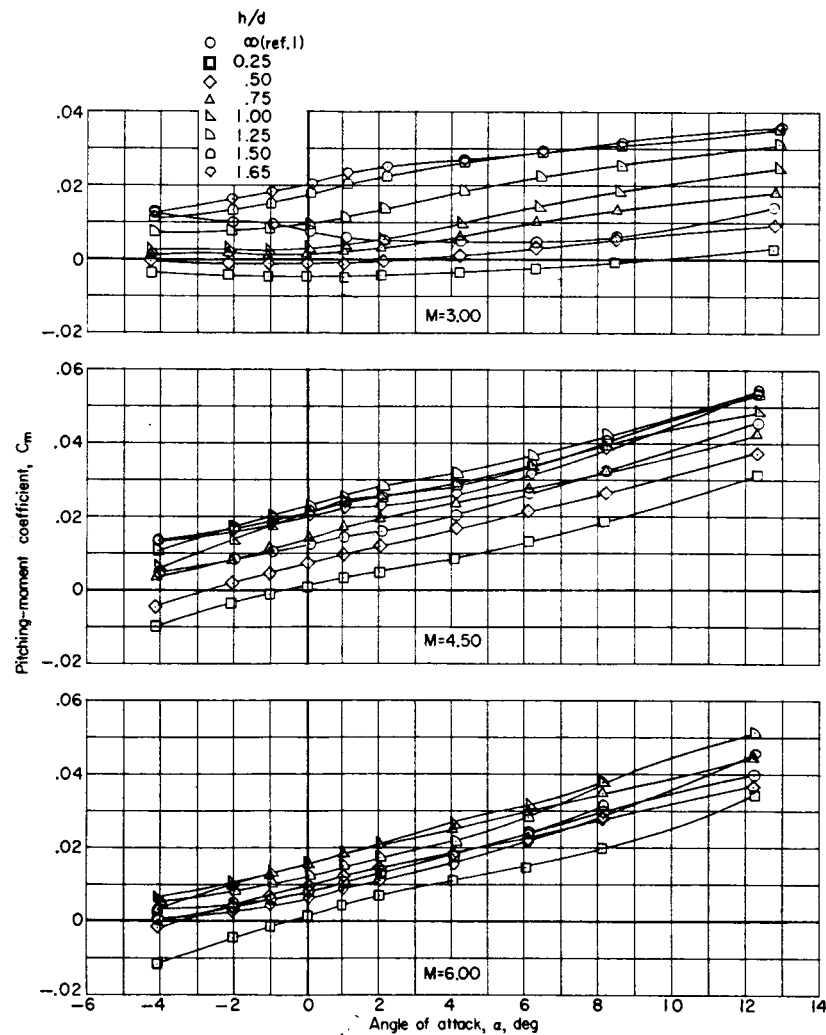


(a) Variation of lift coefficient with angle of attack.

Figure 5.- Longitudinal aerodynamic characteristics of the first-stage reusable booster in presence of BMS.

UNCLASSIFIED

UNCLASSIFIED  
CONFIDENTIAL



(b) Variation of pitching-moment coefficient with angle of attack.

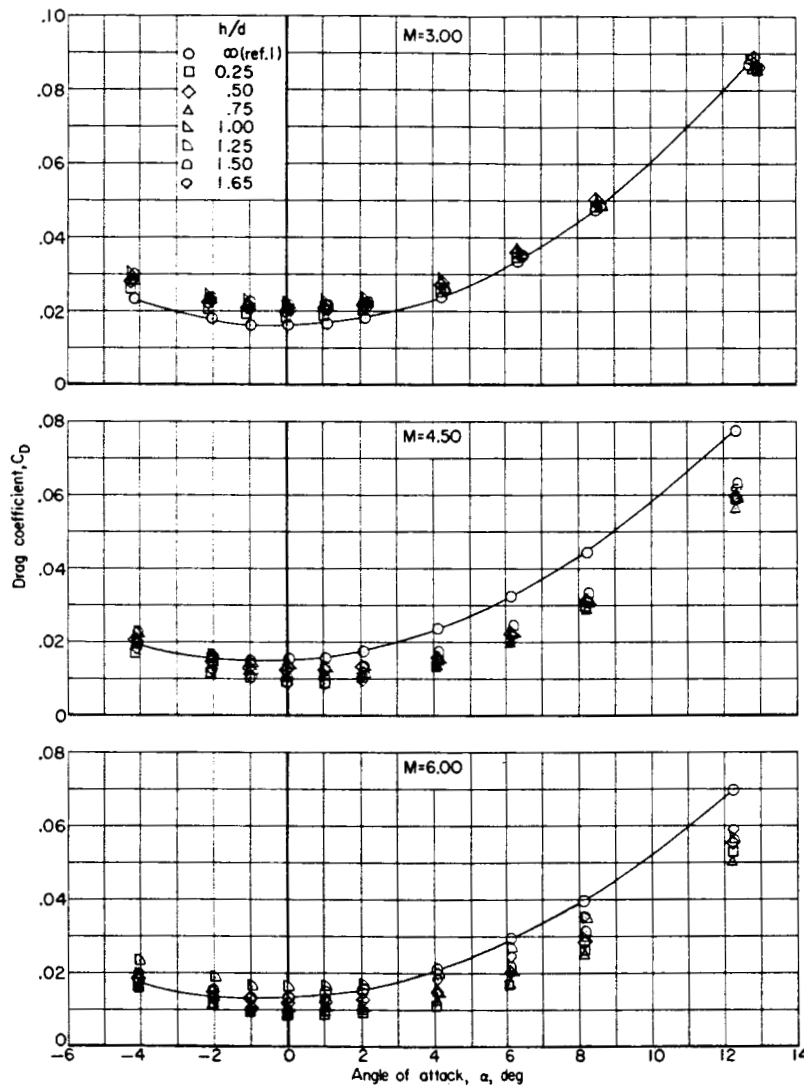
Figure 5.- Continued.

CONFIDENTIAL

UNCLASSIFIED

UNCLASSIFIED

~~CONFIDENTIAL~~



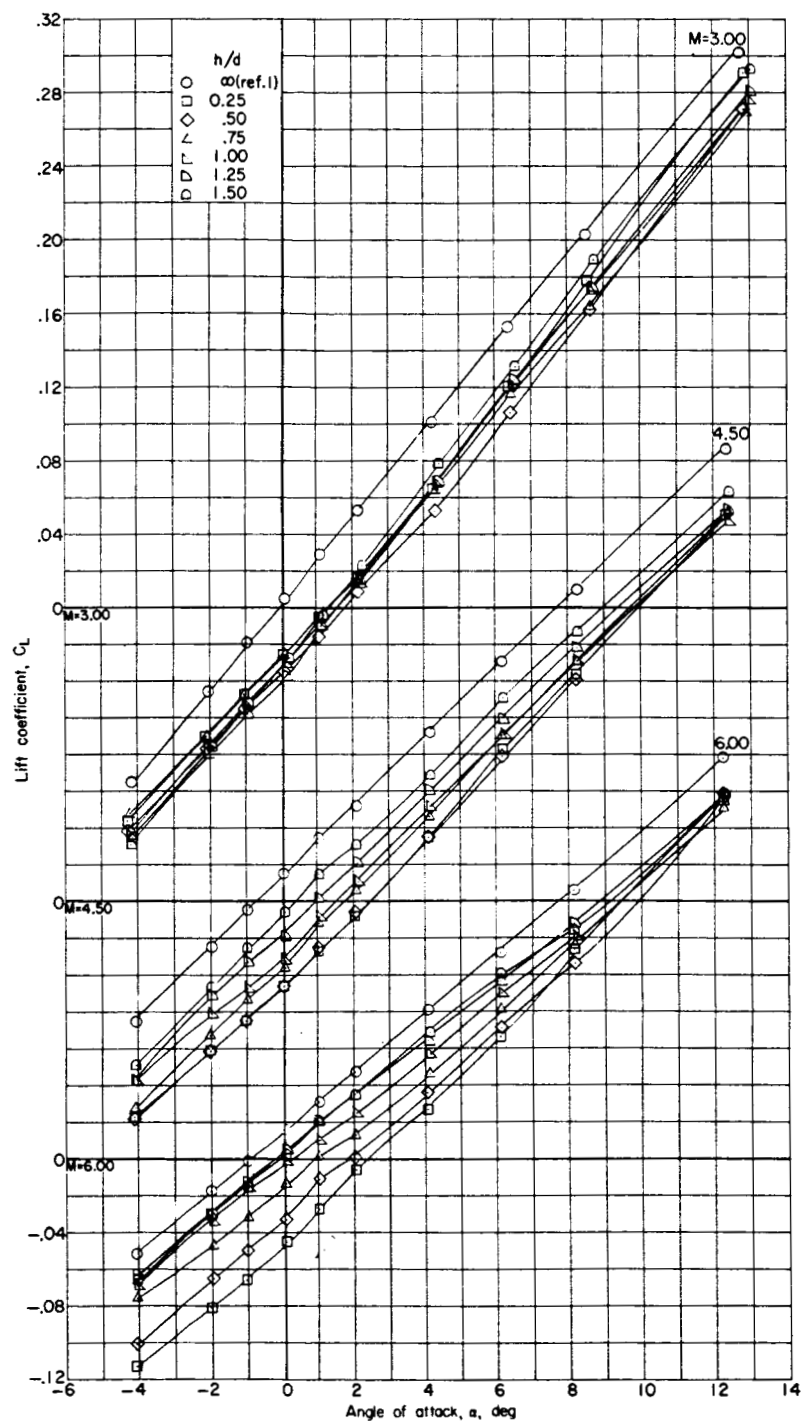
(c) Variation of drag coefficient with angle of attack.

Figure 5.- Concluded.

~~CONFIDENTIAL~~

UNCLASSIFIED

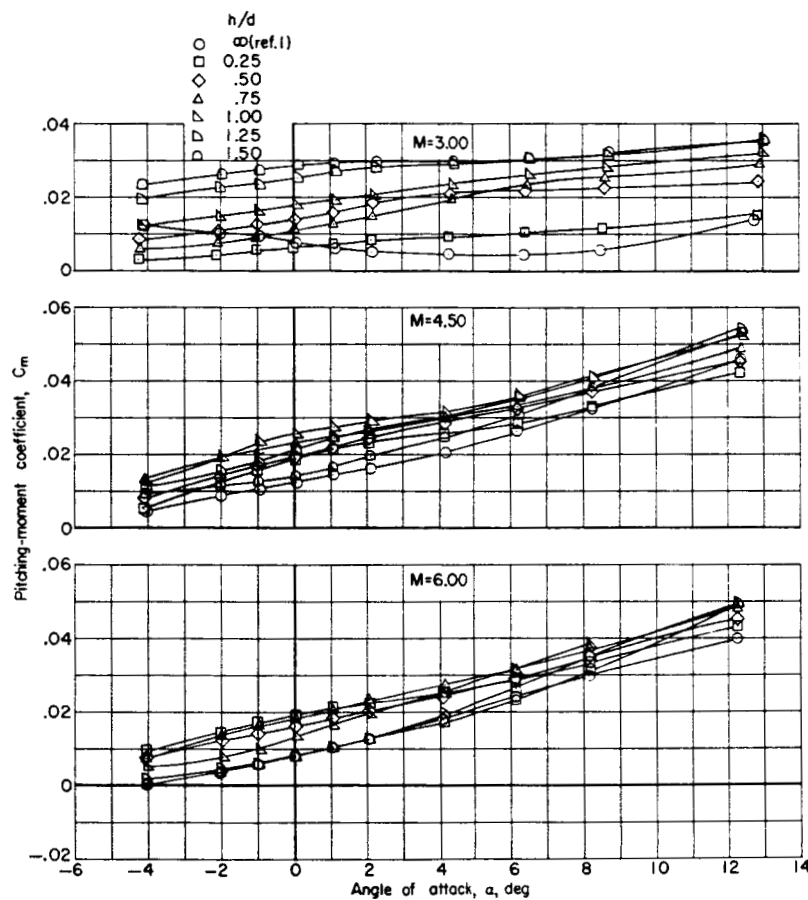
UNCLASSIFIED  
CONFIDENTIAL



(a) Variation of lift coefficient with angle of attack.

Figure 6.- Longitudinal aerodynamic characteristics of the first-stage reusable booster in presence of BWFS.

UNCLASSIFIED  
~~CONFIDENTIAL~~



(b) Variation of pitching-moment coefficient with angle of attack.

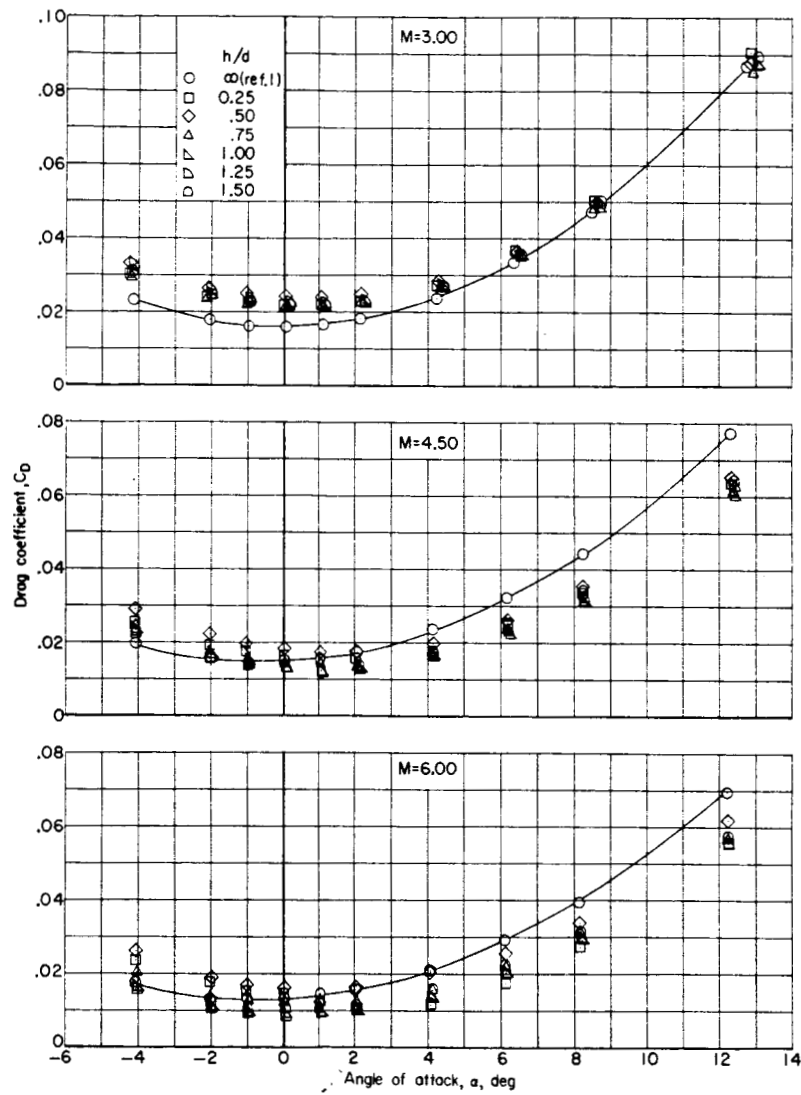
Figure 6.- Continued.

~~CONFIDENTIAL~~

UNCLASSIFIED

UNCLASSIFIED

~~CONFIDENTIAL~~



(c) Variation of drag coefficient with angle of attack.

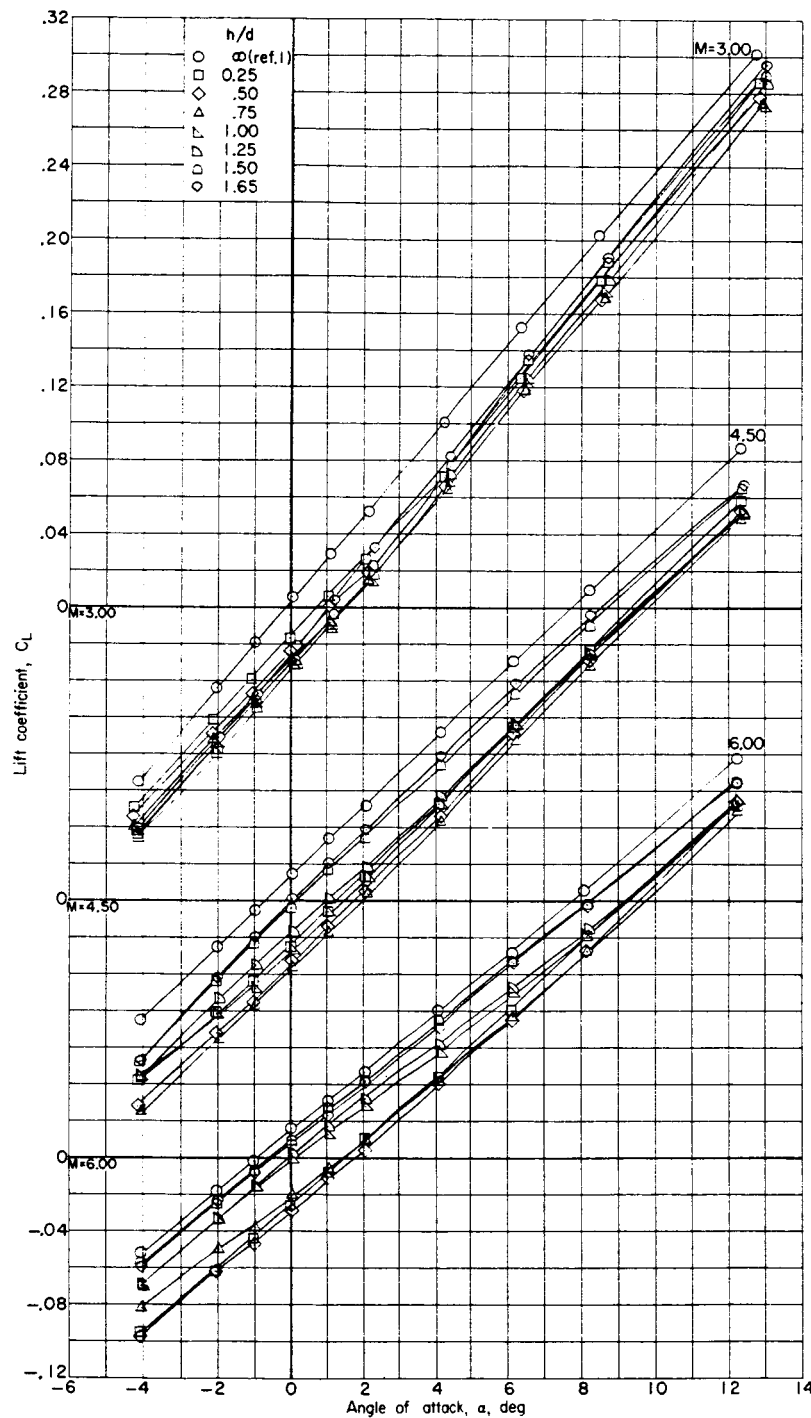
Figure 6.- Concluded.

~~CONFIDENTIAL~~

UNCLASSIFIED

UNCLASSIFIED

~~CONFIDENTIAL~~



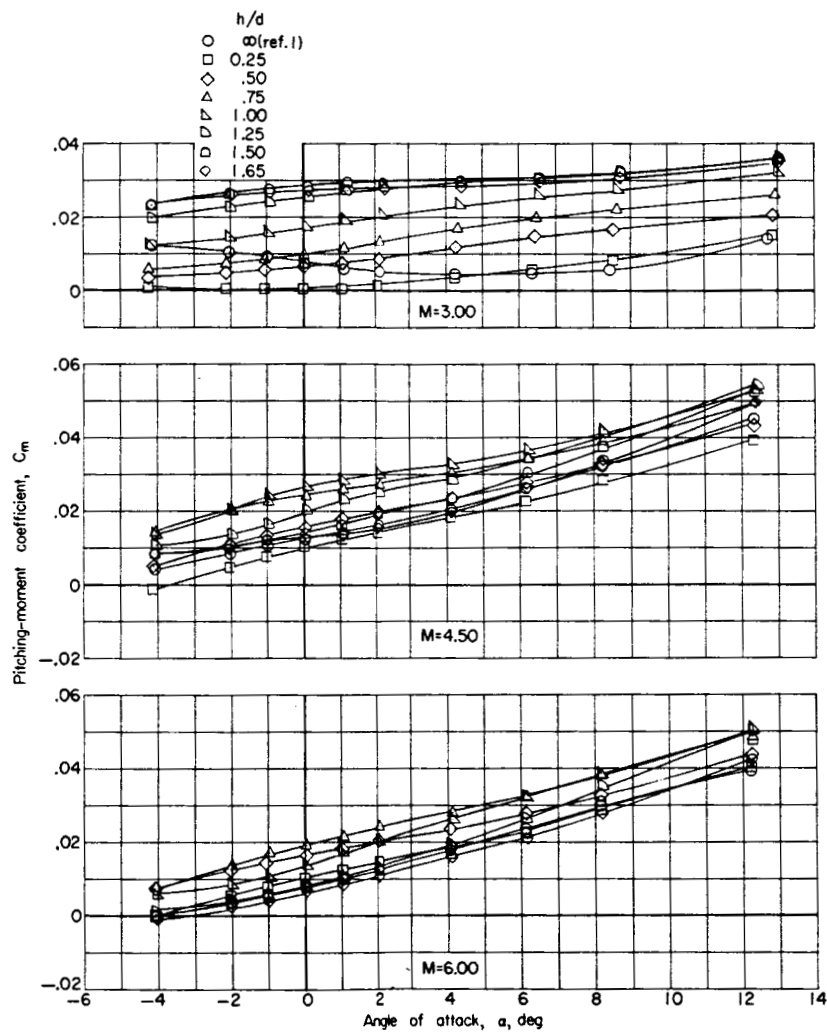
(a) Variation of lift coefficient with angle of attack.

Figure 7.- Longitudinal aerodynamic characteristics of the first-stage reusable booster in presence of BS.

~~CONFIDENTIAL~~

UNCLASSIFIED

UNCLASSIFIED  
CONFIDENTIAL



(b) Variation of pitching-moment coefficient with angle of attack.

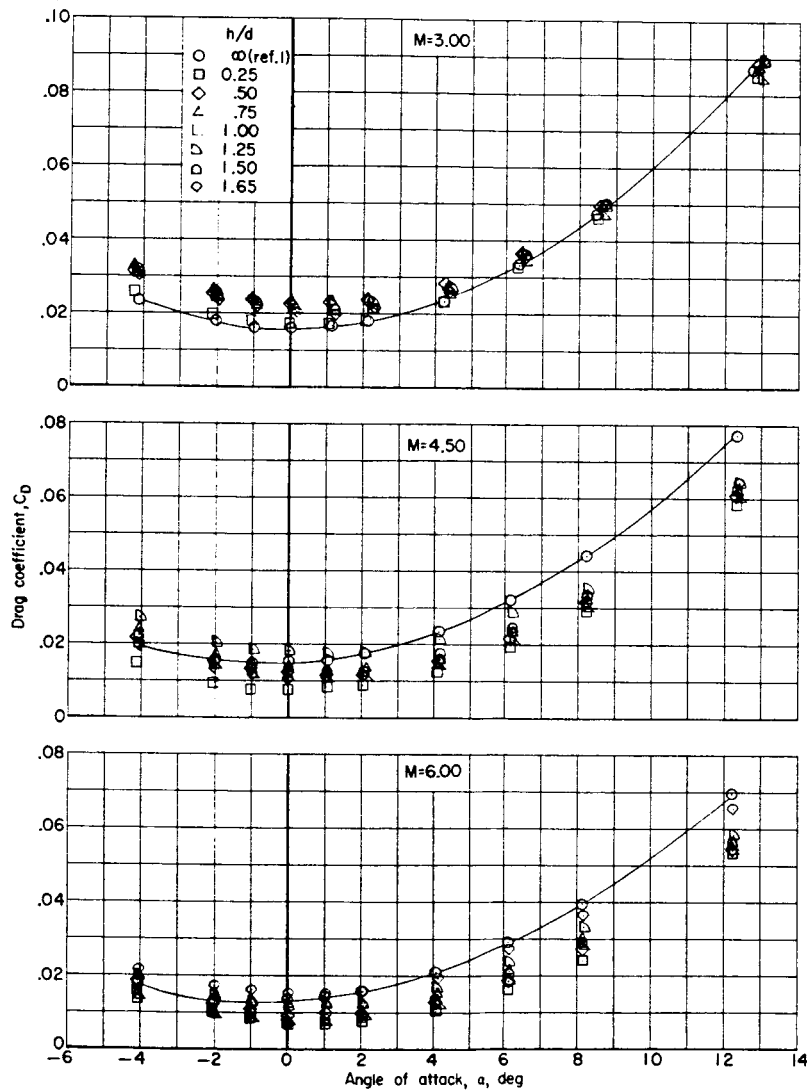
Figure 7.- Continued.

CONFIDENTIAL

UNCLASSIFIED

UNCLASSIFIED

~~CONFIDENTIAL~~



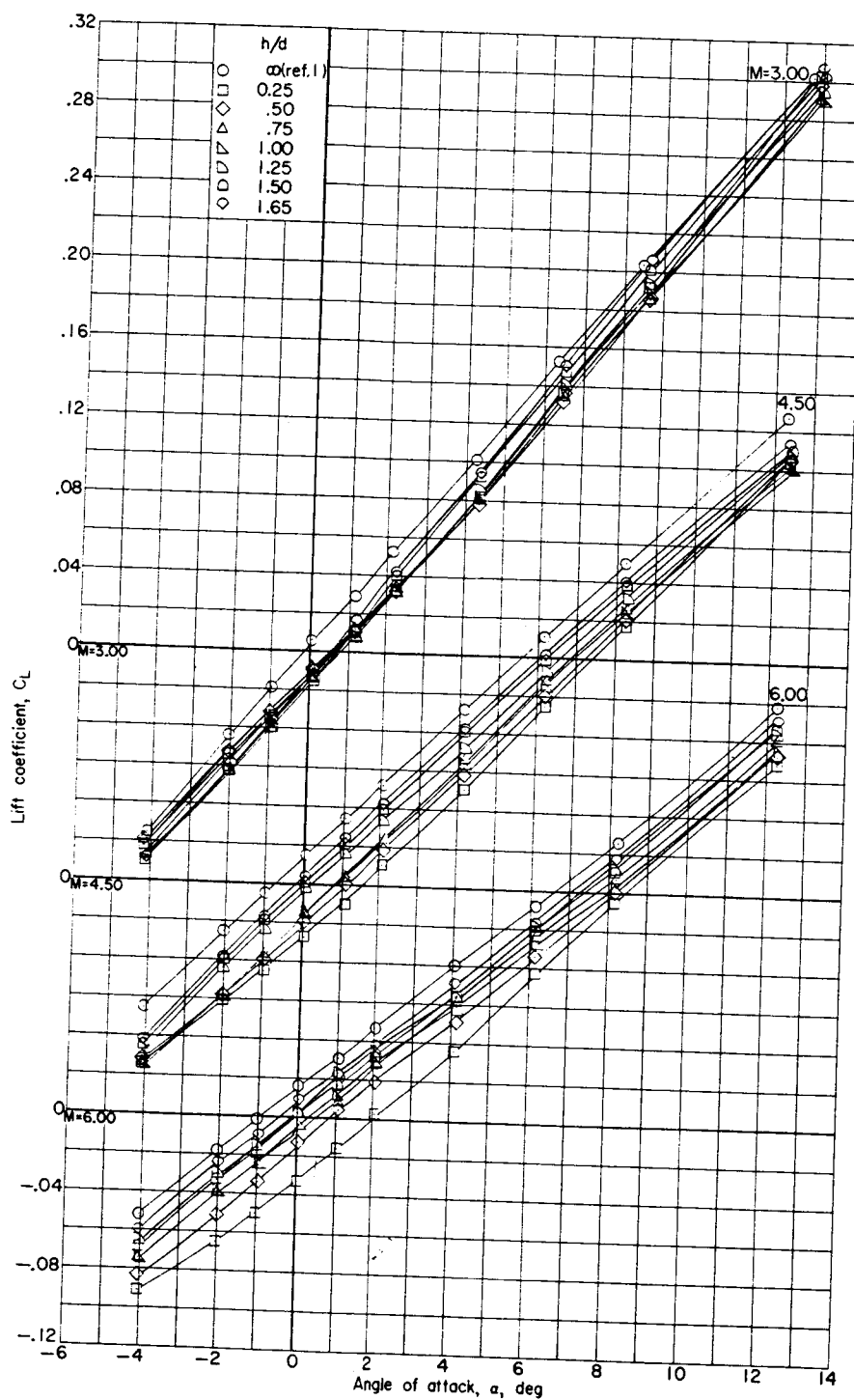
(c) Variation of drag coefficient with angle of attack.

Figure 7.- Concluded.

~~CONFIDENTIAL~~

UNCLASSIFIED

UNCLASSIFIED  
CONFIDENTIAL



(a) Variation with lift coefficient with angle of attack.

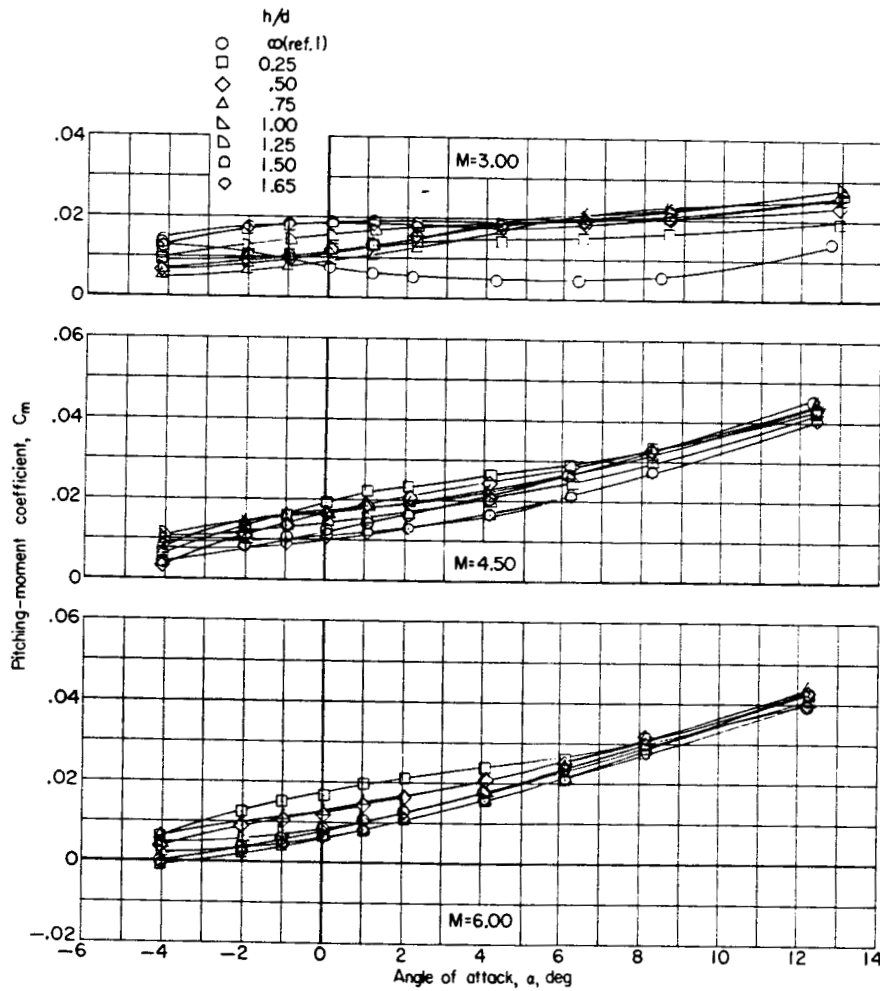
Figure 8.- Longitudinal aerodynamic characteristics of the first-stage reusable booster in presence of BWFS'.

CONFIDENTIAL

UNCLASSIFIED

UNCLASSIFIED

~~CONFIDENTIAL~~



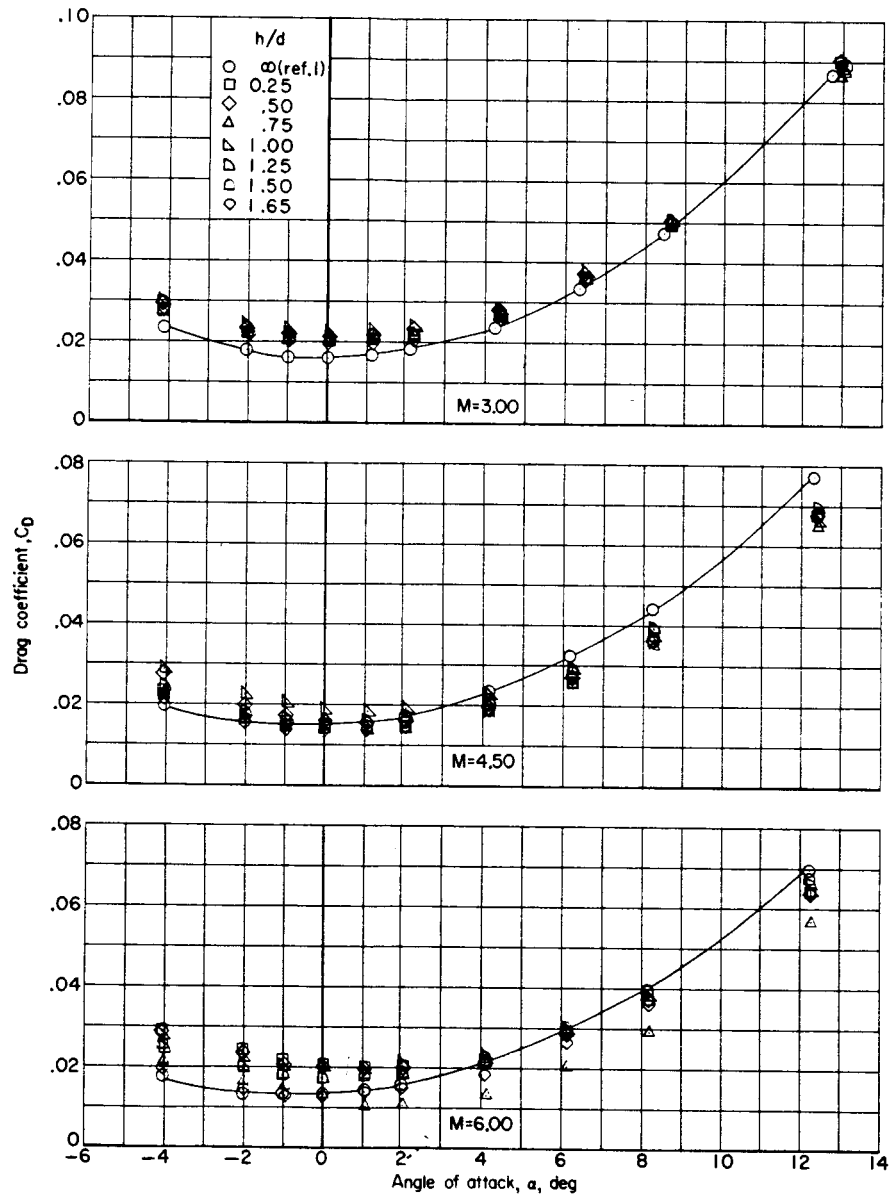
(b) Variation of pitching-moment coefficient with angle of attack.

Figure 8.- Continued.

~~CONFIDENTIAL~~

UNCLASSIFIED

UNCLASSIFIED  
CONFIDENTIAL



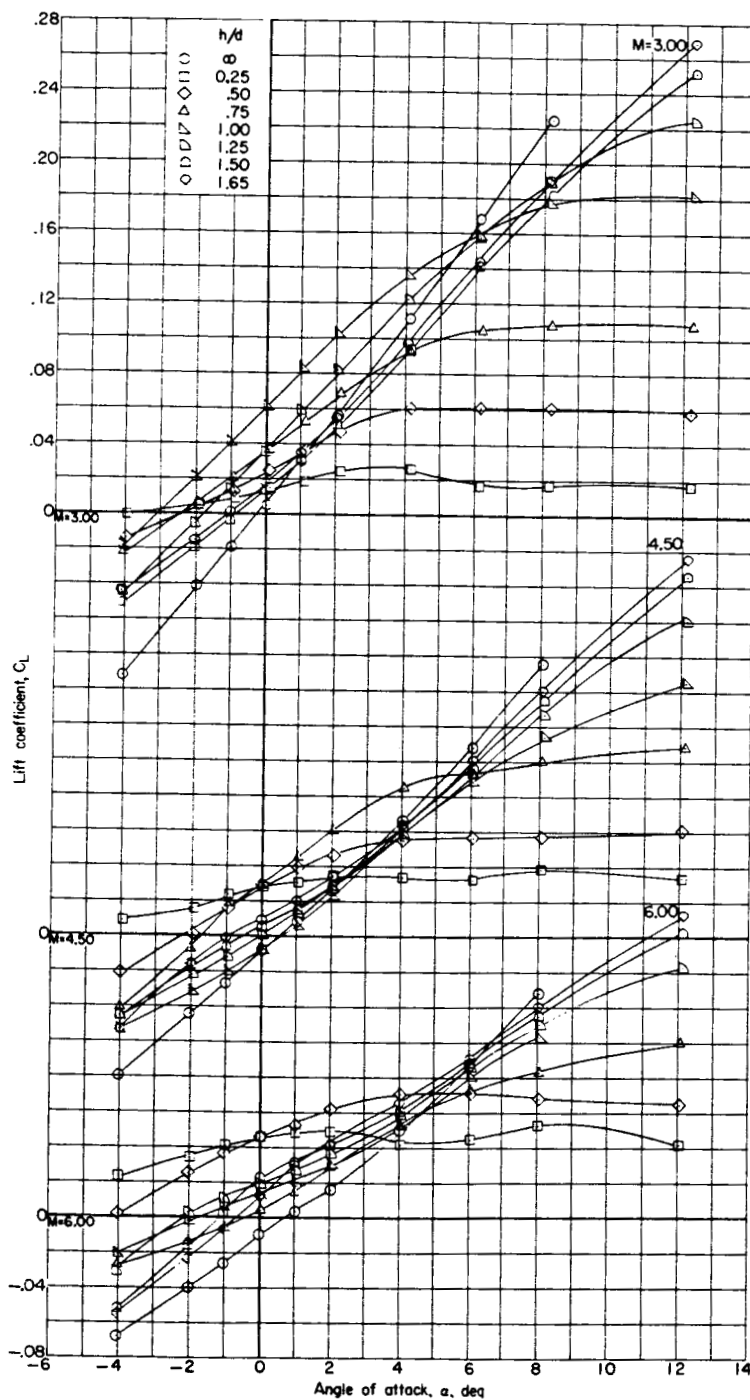
(c) Variation of drag coefficient with angle of attack.

Figure 8.- Concluded.

CONFIDENTIAL

UNCLASSIFIED

UNCLASSIFIED



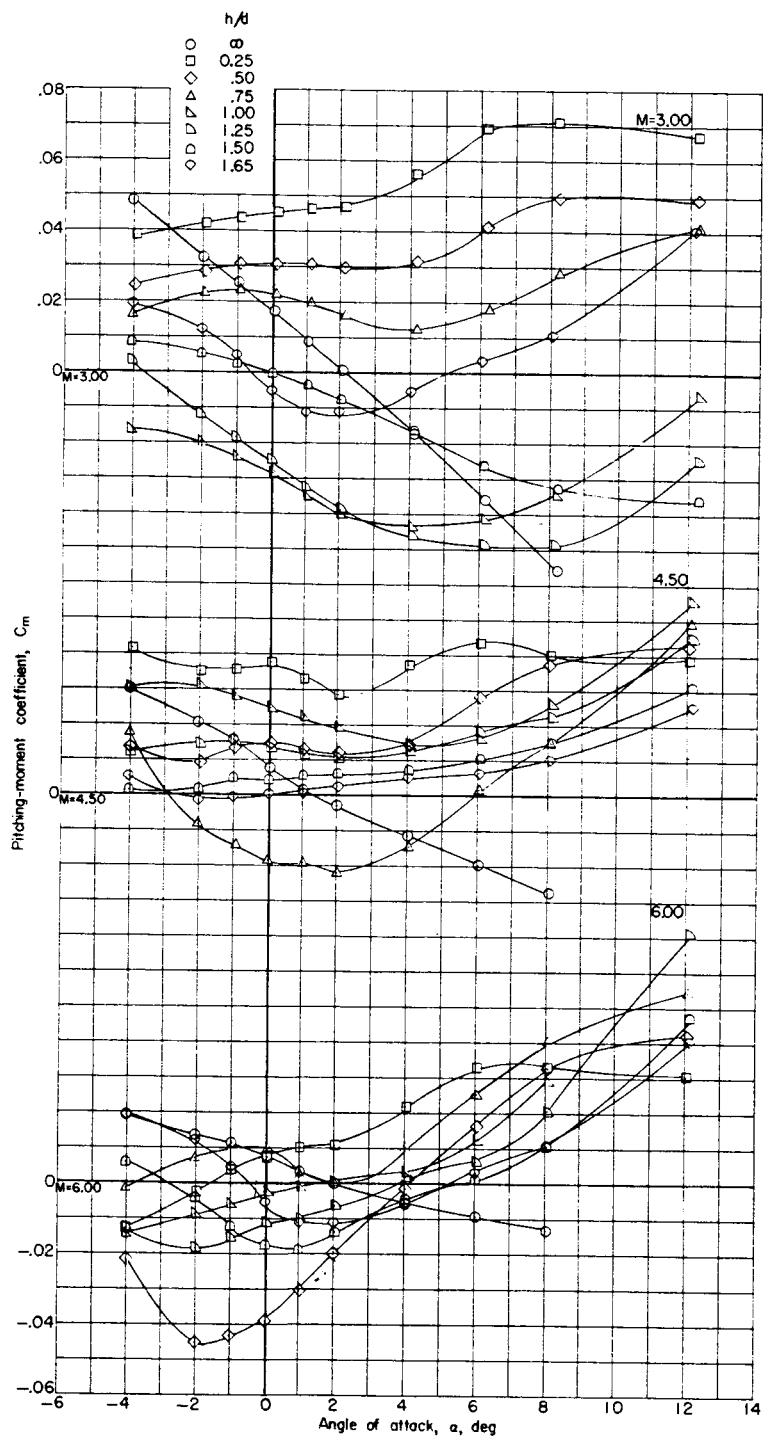
(a) Variation of lift coefficient with angle of attack.

Figure 9.- Longitudinal aerodynamic characteristics of BWFS in presence of the first-stage reusable booster.

UNCLASSIFIED

UNCLASSIFIED

UNCLASSIFIED  
CONFIDENTIAL



(b) Variation of pitching-moment coefficient with angle of attack.

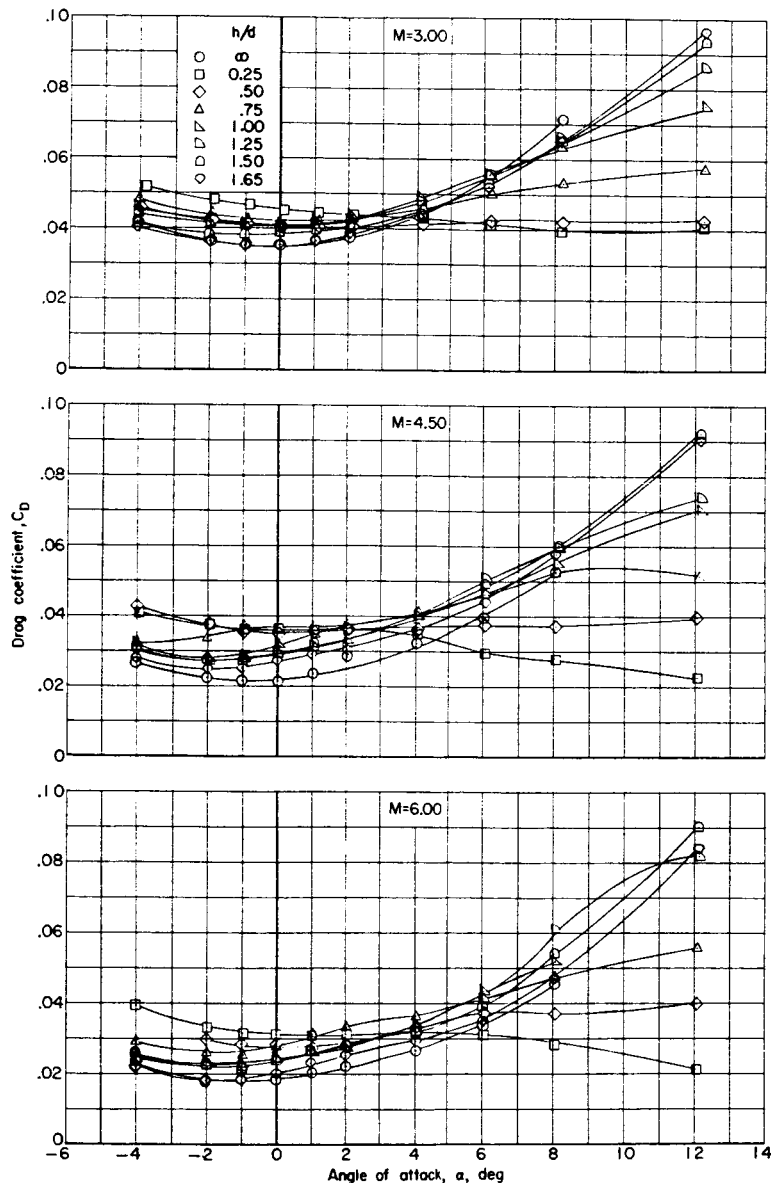
Figure 9.- Continued.

CONFIDENTIAL

UNCLASSIFIED

UNCLASSIFIED

~~CONFIDENTIAL~~



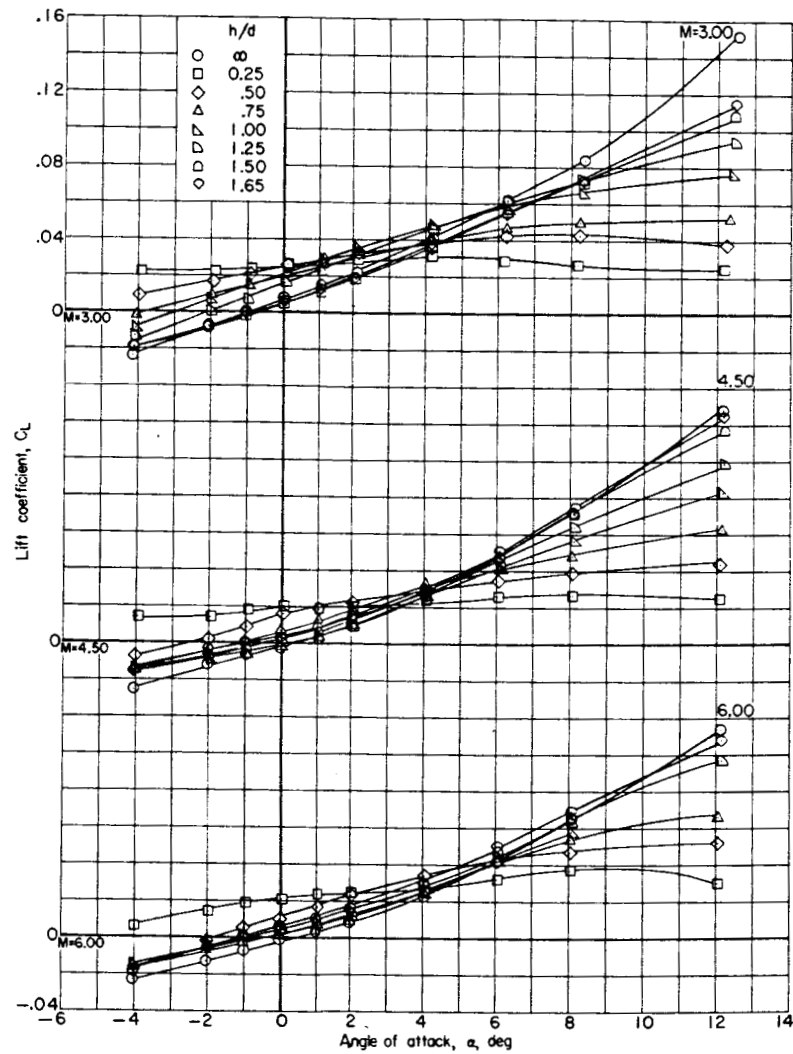
(c) Variation of drag coefficient with angle of attack.

Figure 9.- Concluded.

~~CONFIDENTIAL~~

UNCLASSIFIED

UNCLASSIFIED

~~CONFIDENTIAL~~

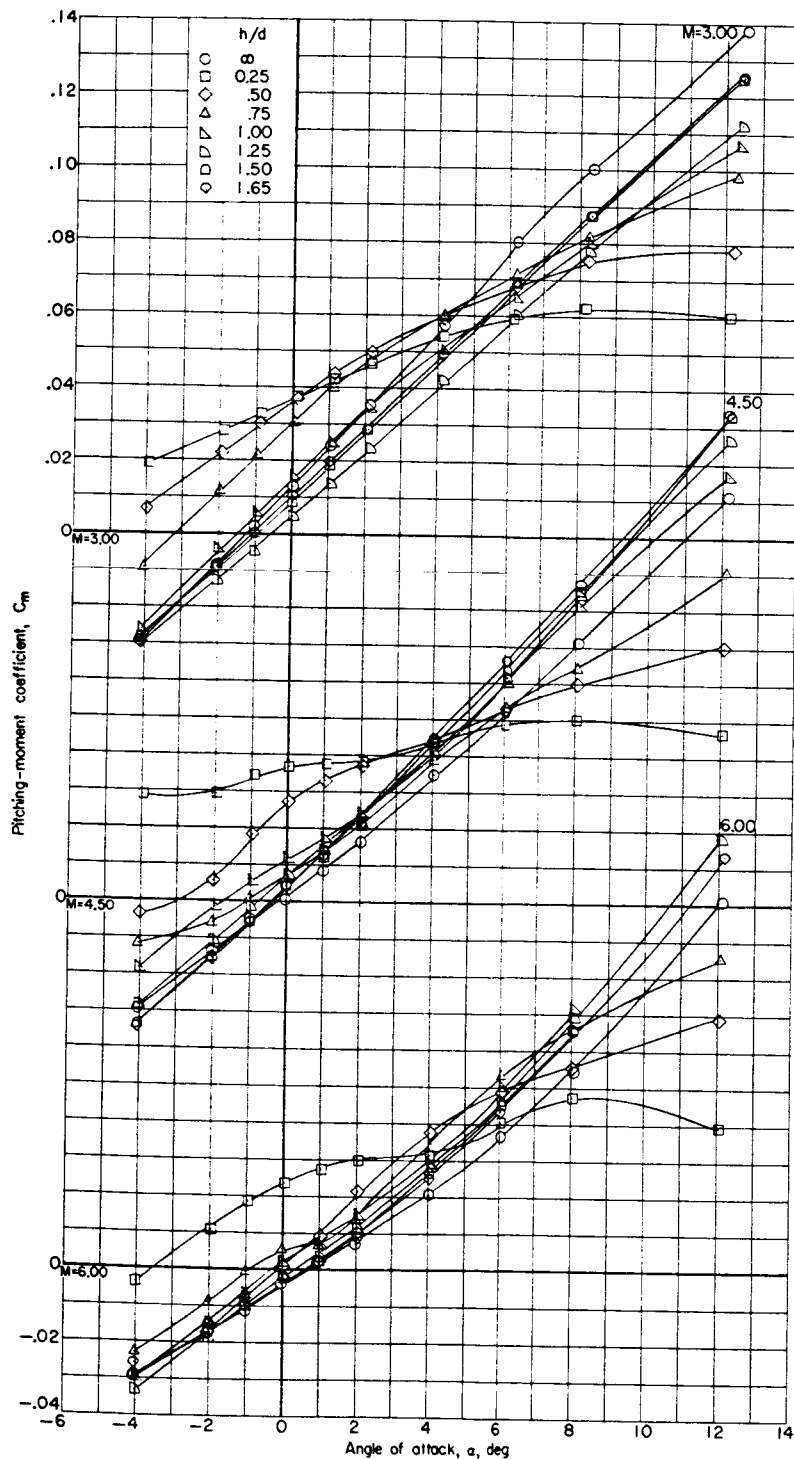
(a) Variation of lift coefficient with angle of attack.

Figure 10.- Longitudinal aerodynamic characteristics of BMS in presence of the first-stage reusable booster.

UNCLASSIFIED

UNCLASSIFIED

~~CONFIDENTIAL~~



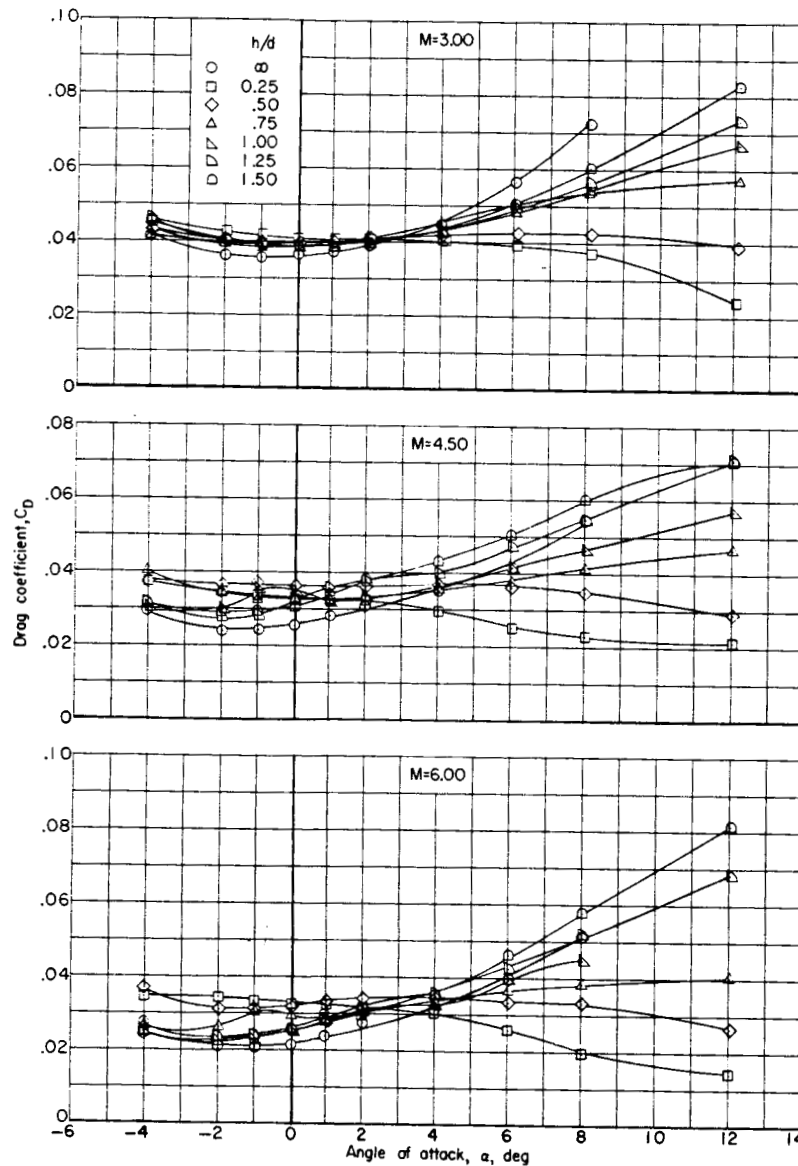
(b) Variation of pitching-moment coefficient with angle of attack.

Figure 10.- Continued.

~~CONFIDENTIAL~~

UNCLASSIFIED

UNCLASSIFIED  
~~CONFIDENTIAL~~



(c) Variation of drag coefficient with angle of attack.

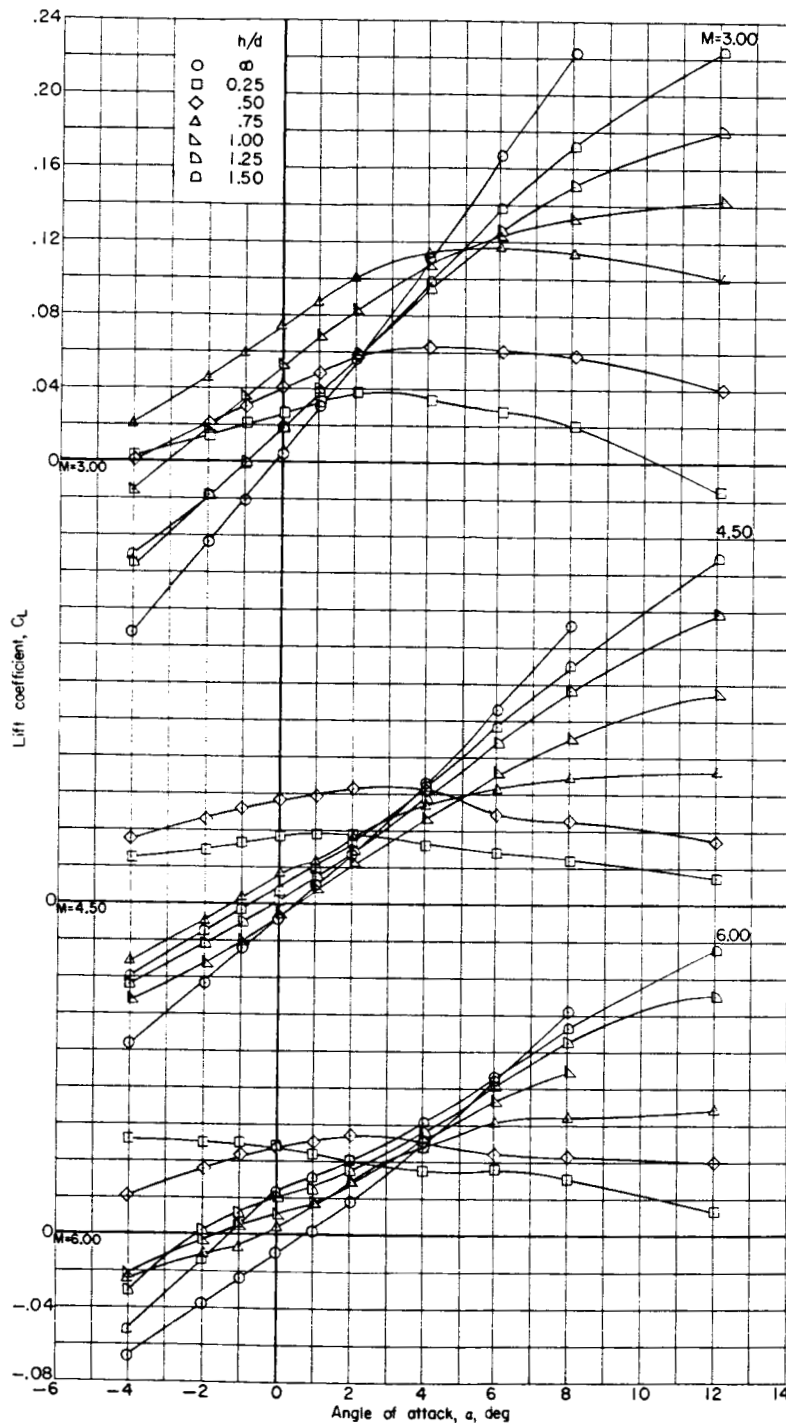
Figure 10.- Concluded.

~~CONFIDENTIAL~~

UNCLASSIFIED

UNCLASSIFIED

~~CONFIDENTIAL~~



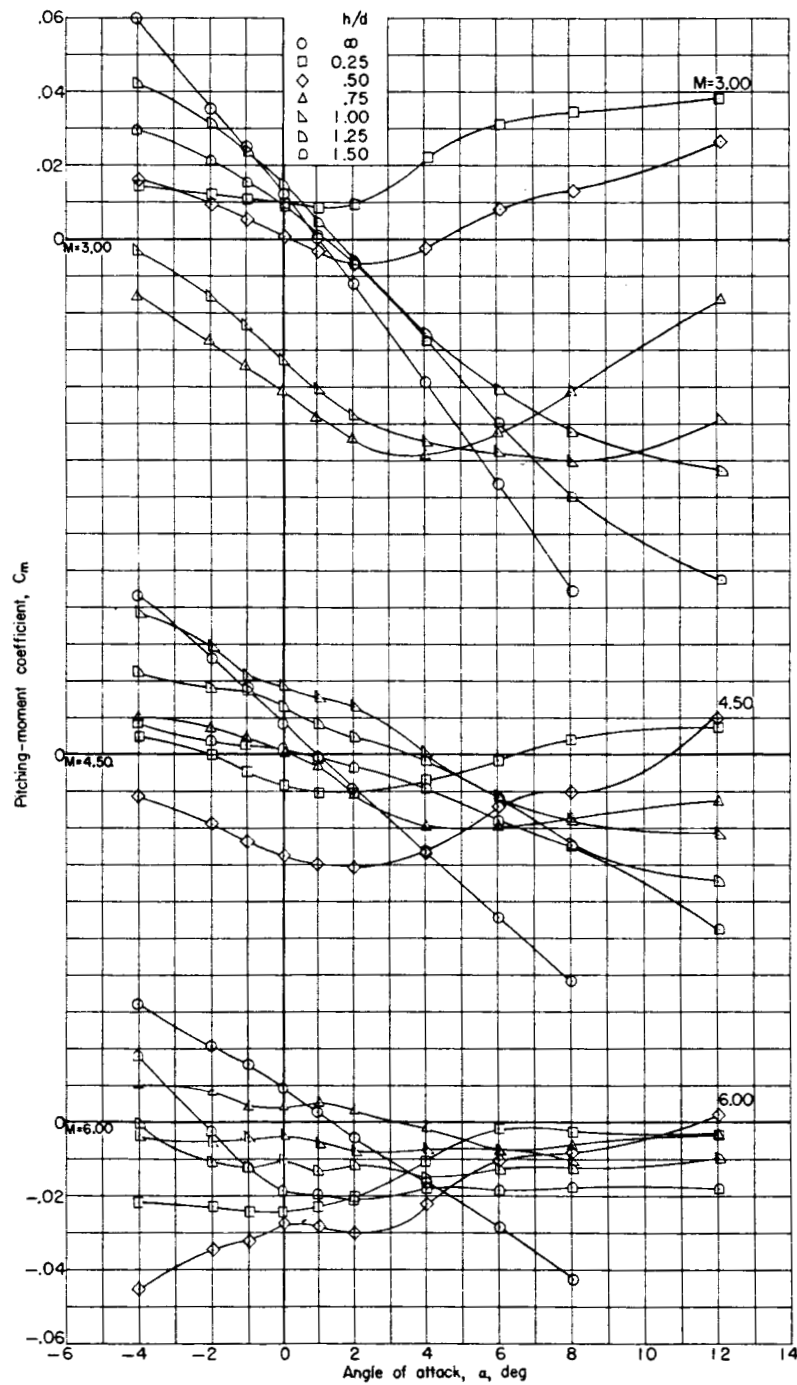
(a) Variation of lift coefficient with angle of attack.

Figure 11.- Longitudinal aerodynamic characteristics of BWFS in presence of the first-stage reusable booster.

~~CONFIDENTIAL~~

UNCLASSIFIED

UNCLASSIFIED  
CONFIDENTIAL



(b) Variation of pitching-moment coefficient with angle of attack.

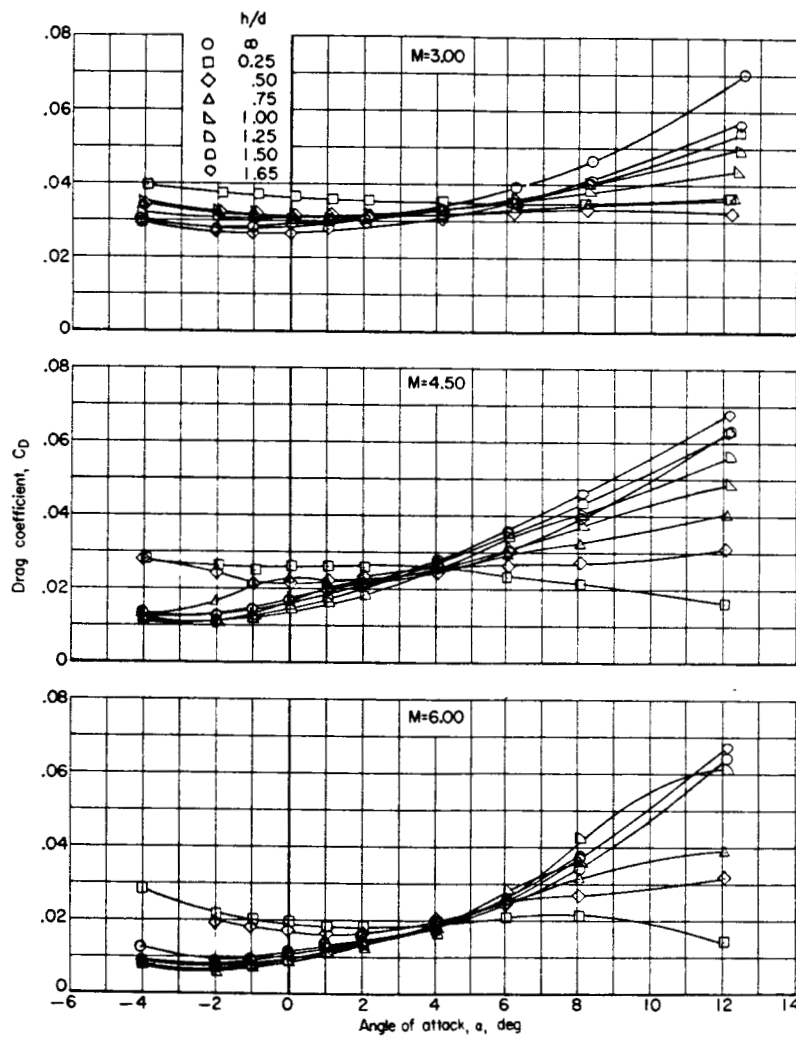
Figure 11.- Continued.

CONFIDENTIAL

UNCLASSIFIED

UNCLASSIFIED

~~CONFIDENTIAL~~



(c) Variation of drag coefficient with angle of attack.

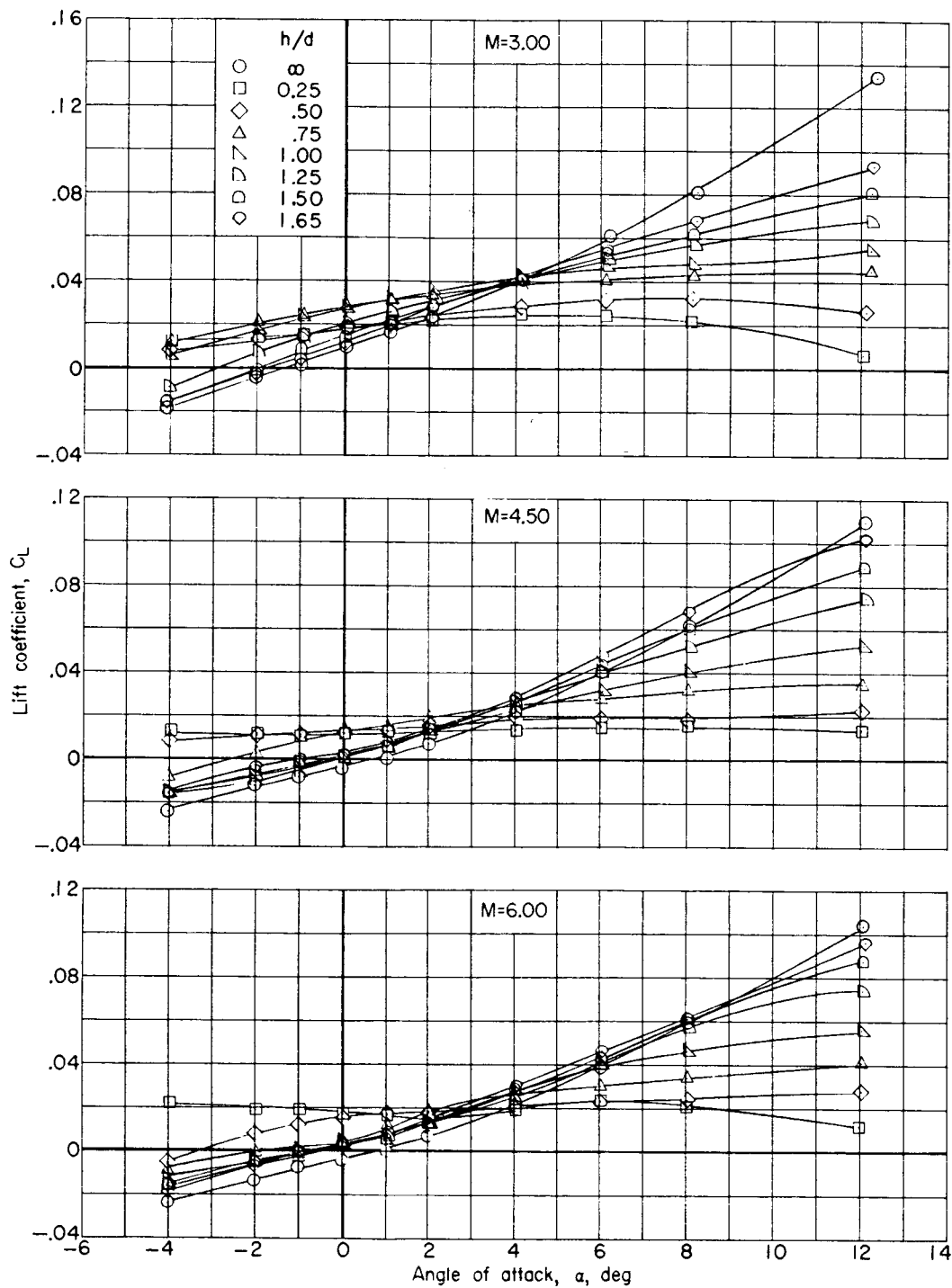
Figure 11.- Concluded.

~~CONFIDENTIAL~~

UNCLASSIFIED

UNCLASSIFIED

~~CONFIDENTIAL~~



(a) Variation of lift coefficient with angle of attack.

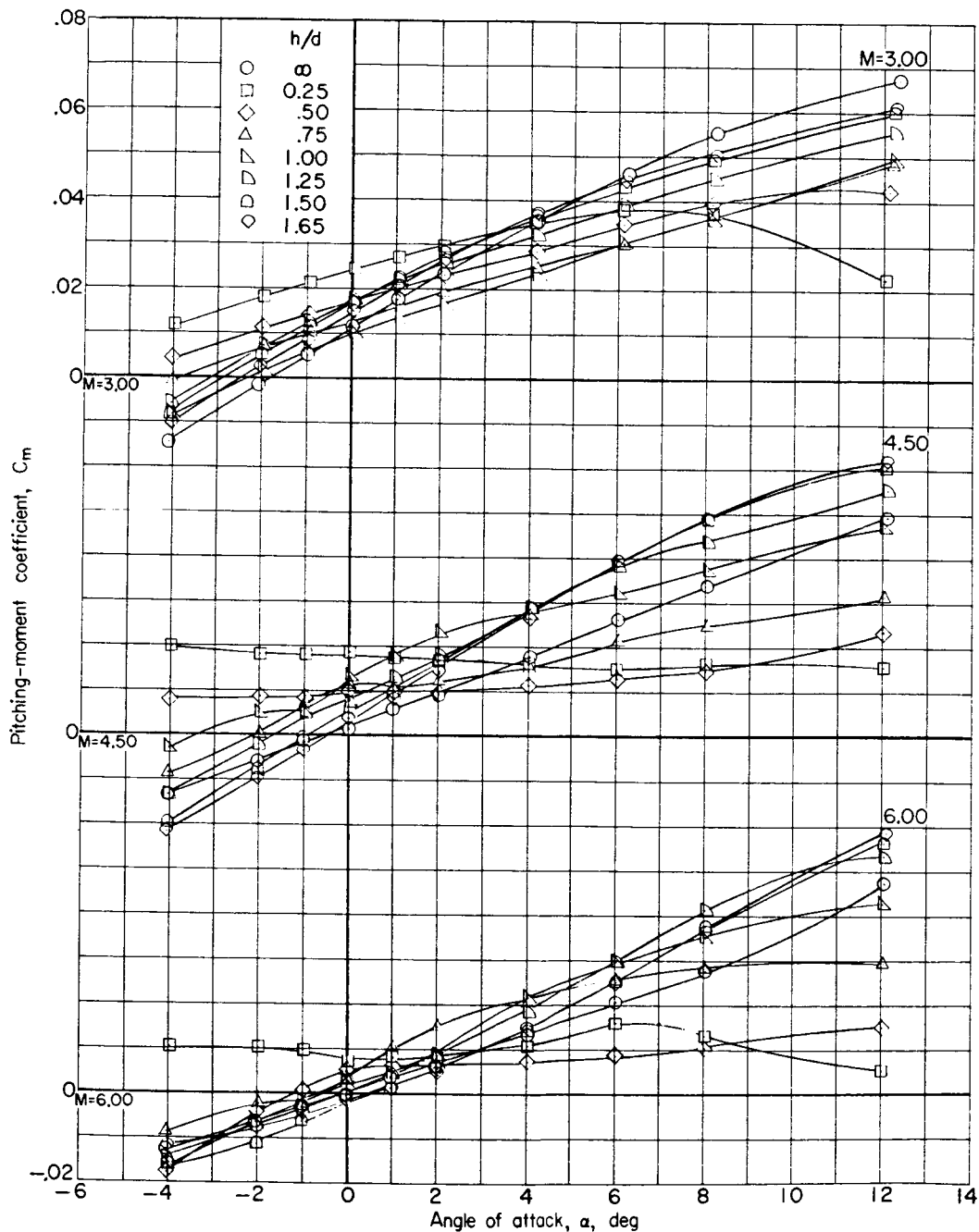
Figure 12.- Longitudinal aerodynamic characteristics of BS in presence of the first-stage reusable booster.

~~CONFIDENTIAL~~

UNCLASSIFIED

UNCLASSIFIED

~~CONFIDENTIAL~~



(b) Variation of pitching-moment coefficient with angle of attack.

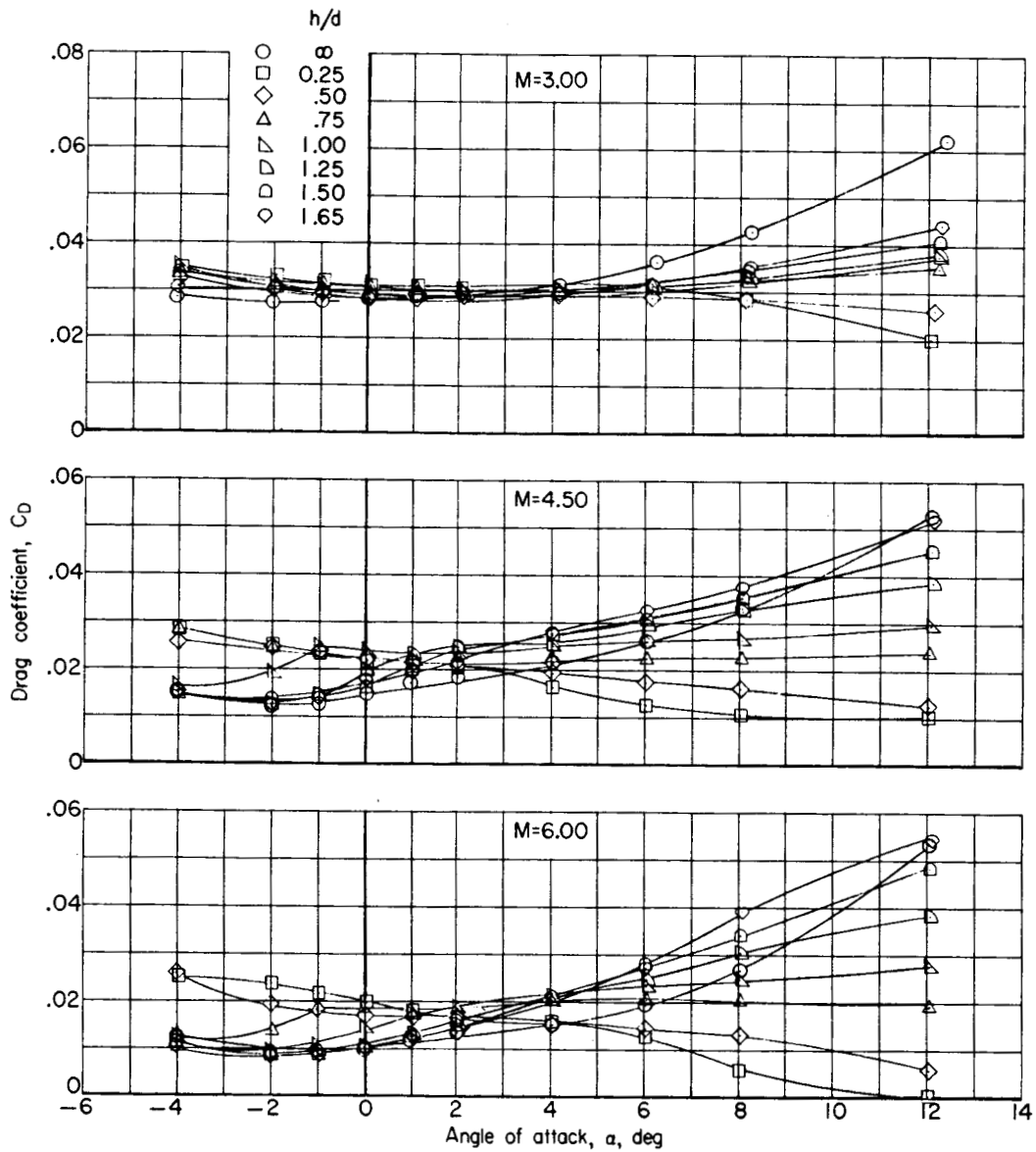
Figure 12.- Continued.

~~CONFIDENTIAL~~

UNCLASSIFIED

UNCLASSIFIED

~~CONFIDENTIAL~~



(c) Variation of drag coefficient with angle of attack.

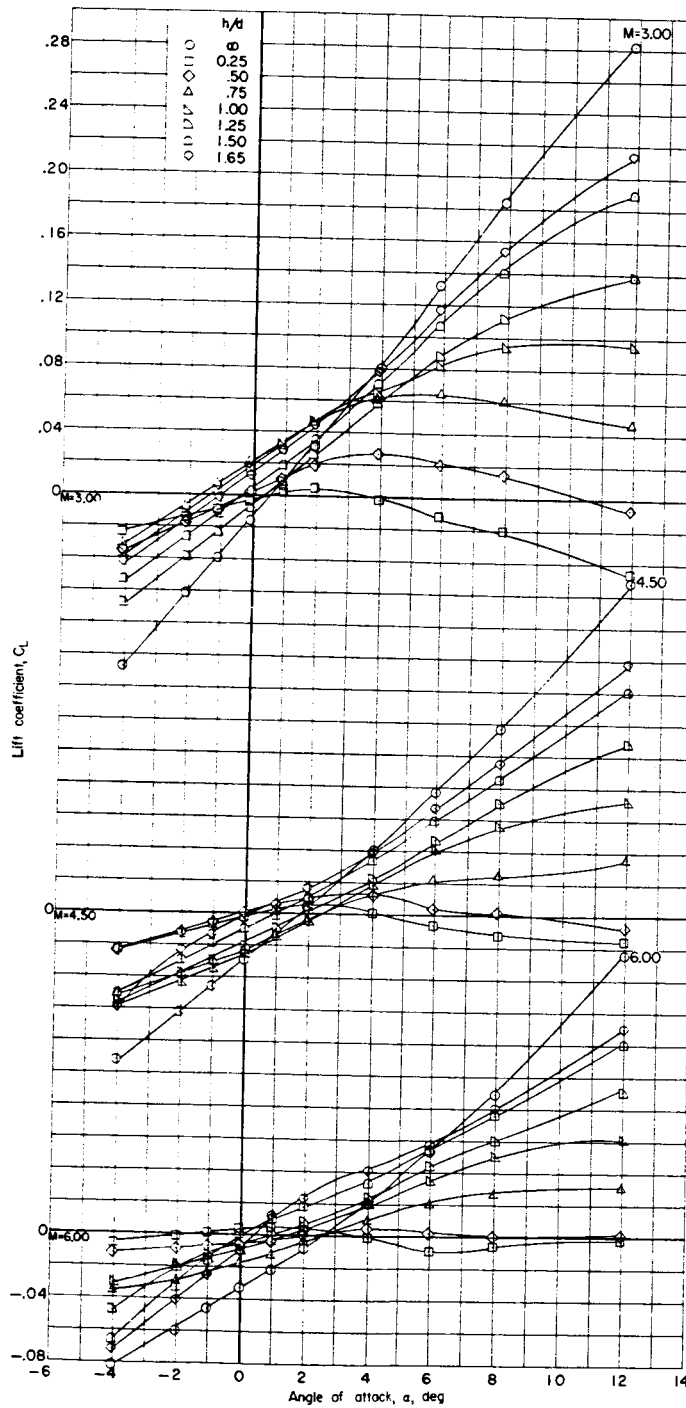
Figure 12.- Concluded.

~~CONFIDENTIAL~~

UNCLASSIFIED

UNCLASSIFIED

~~CONFIDENTIAL~~



(a) Variation of lift coefficient with angle of attack.

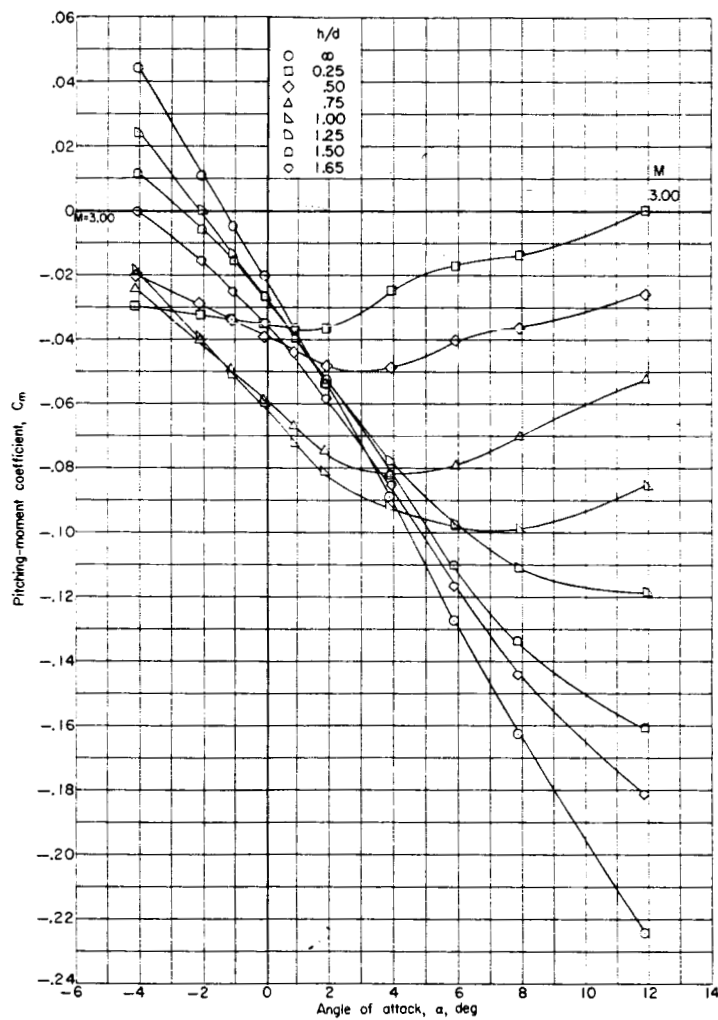
Figure 13.- Longitudinal aerodynamic characteristics of BWFS' in presence of the first-stage reusable booster.

~~CONFIDENTIAL~~

UNCLASSIFIED

UNCLASSIFIED

~~CONFIDENTIAL~~



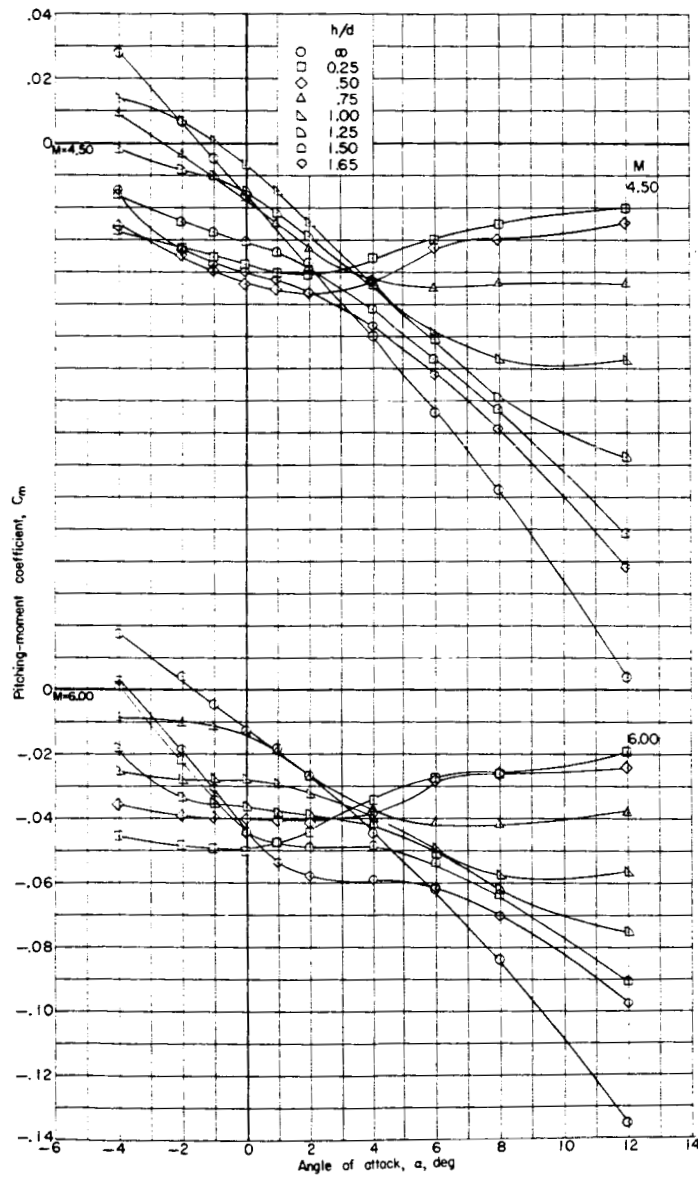
(b) Variation of pitching-moment coefficient with angle of attack.

Figure 13.- Continued.

~~CONFIDENTIAL~~

UNCLASSIFIED

UNCLASSIFIED  
CONFIDENTIAL



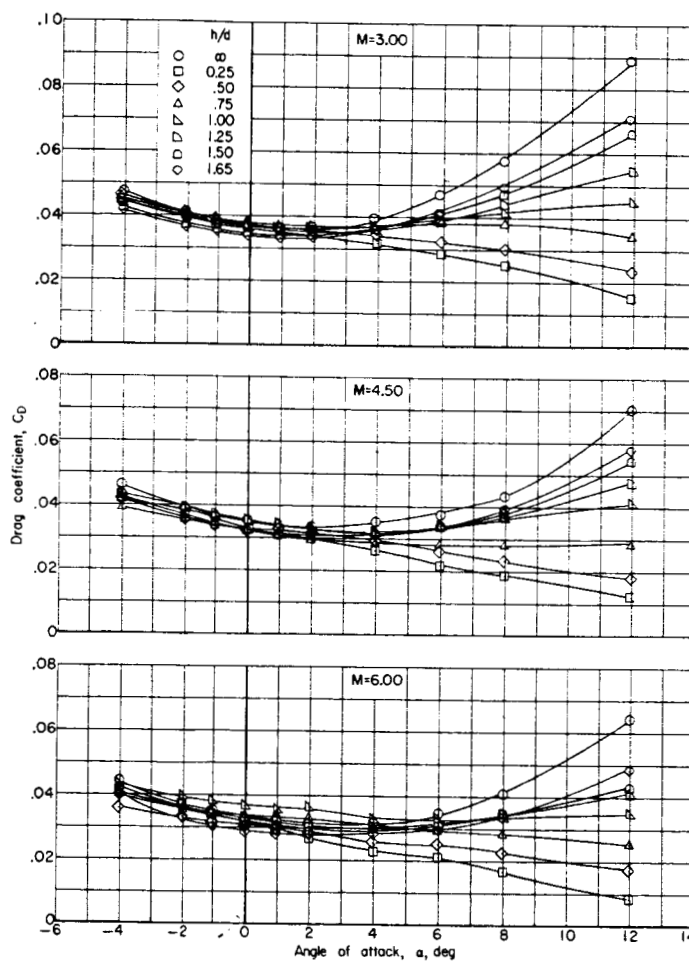
(b) Continued.

Figure 13.- Continued.

CONFIDENTIAL

UNCLASSIFIED

UNCLASSIFIED  
CONFIDENTIAL



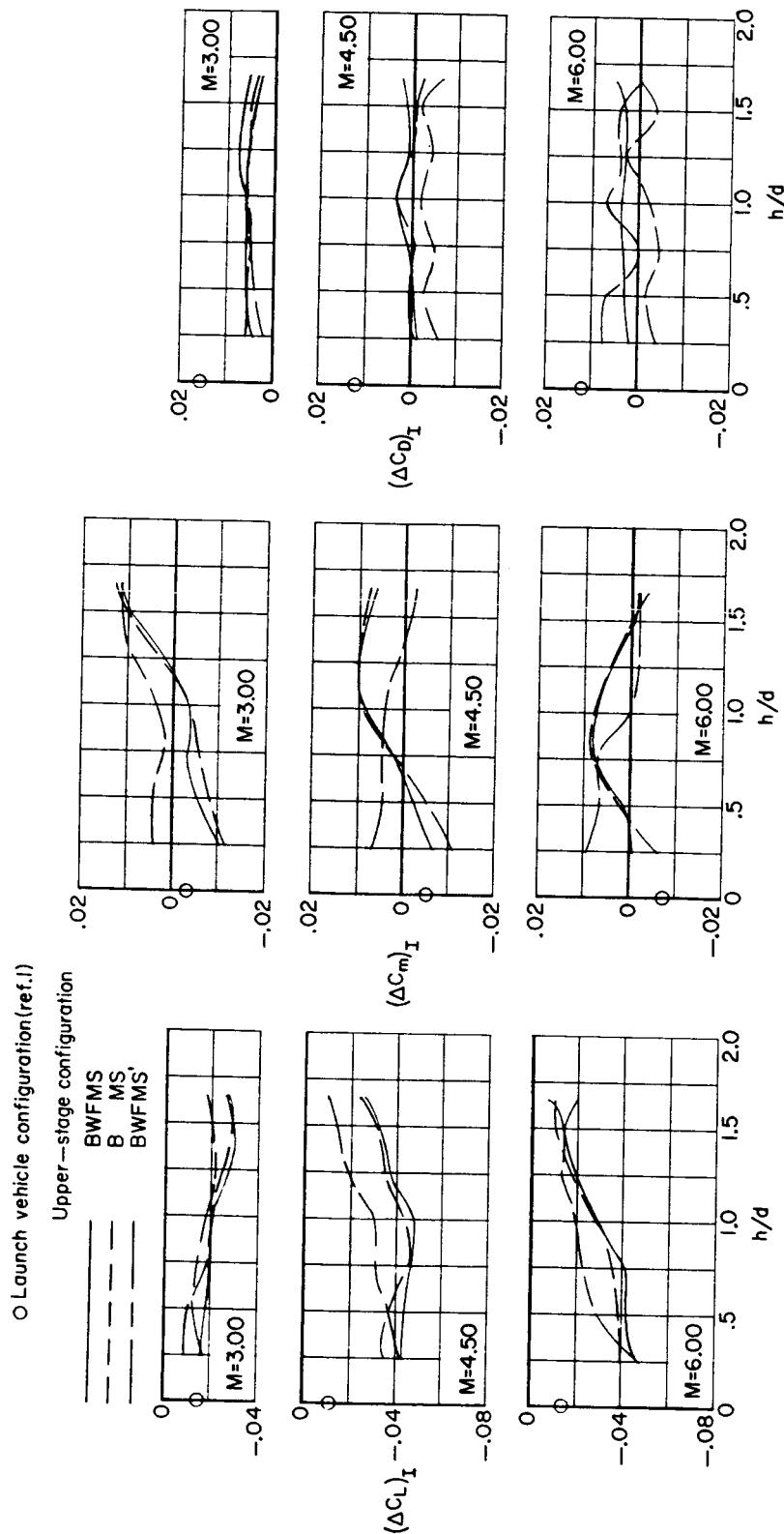
(c) Variation of drag coefficient with angle of attack.

Figure 13.- Concluded.

UNCLASSIFIED

UNCLASSIFIED

CONFIDENTIAL



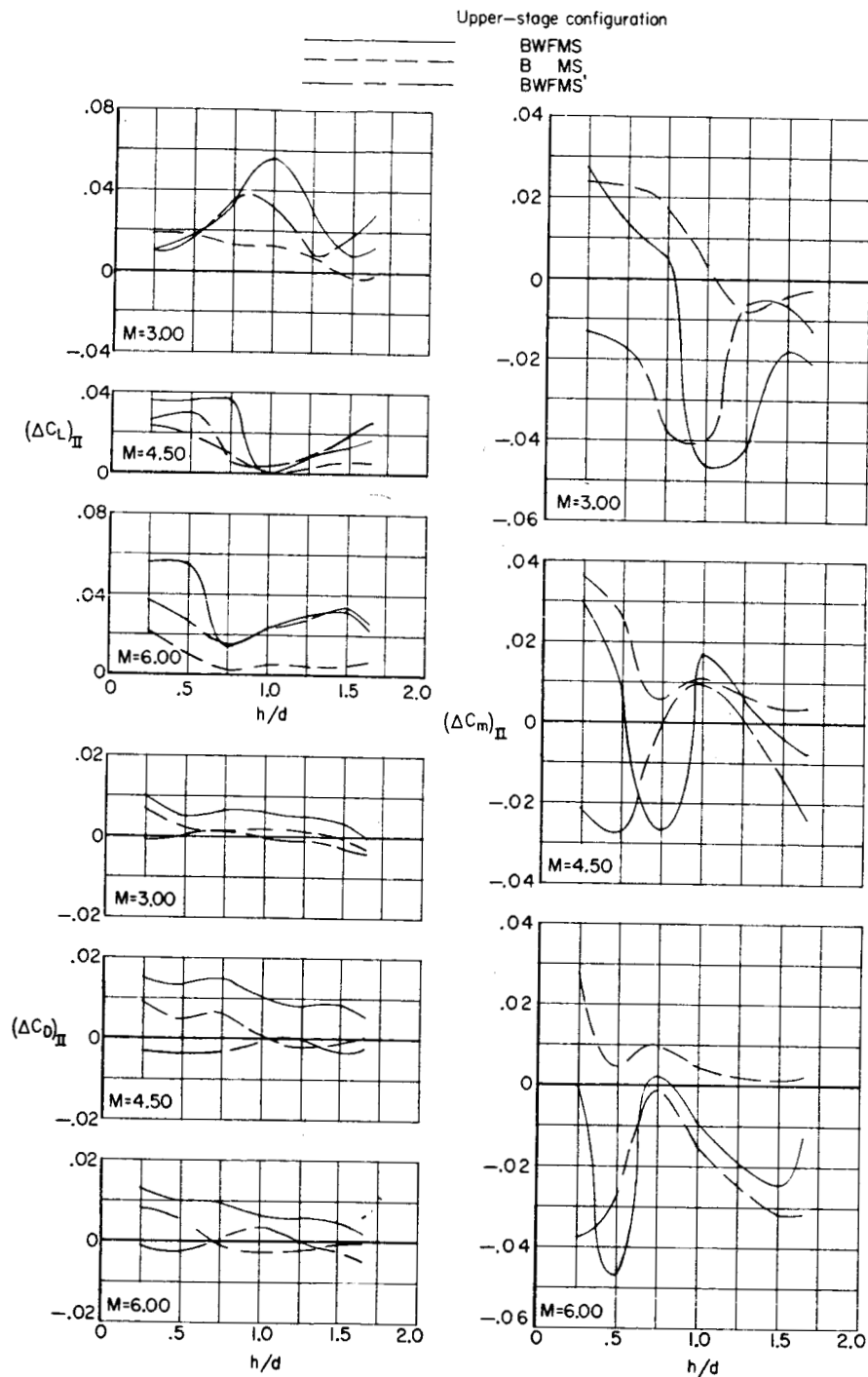
(a) Incremental changes for the first-stage reusable booster in presence of various upper-stage configurations.

Figure 14.- Variation with spacing distance of the incremental changes in lift, pitching moment, and drag coefficient at zero angle of attack for the first-stage reusable booster in presence of various upper-stage configurations and for the various upper-stage configurations in presence of the first stage.

CONFIDENTIAL

UNCLASSIFIED

UNCLASSIFIED

~~CONFIDENTIAL~~

(b) Incremental changes for various upper-stage configurations in presence of the first-stage reusable booster.

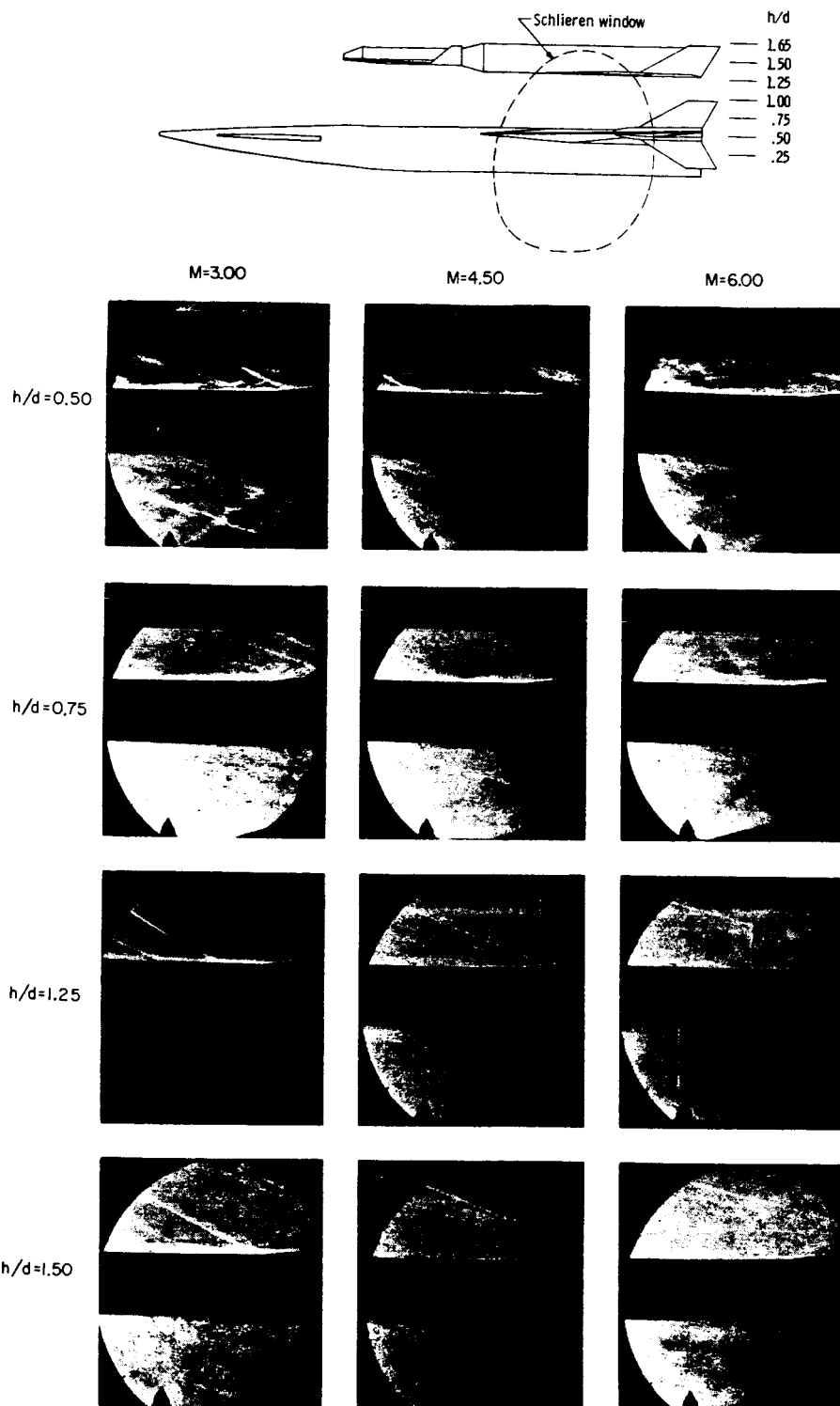
Figure 14.- Concluded.

~~CONFIDENTIAL~~

UNCLASSIFIED

UNCLASSIFIED

~~CONFIDENTIAL~~



L-64-8365

Figure 15.- Schlieren photographs of the first-stage reusable booster in presence of BWFS.

~~CONFIDENTIAL~~

UNCLASSIFIED

UNCLASSIFIED

~~CONFIDENTIAL~~

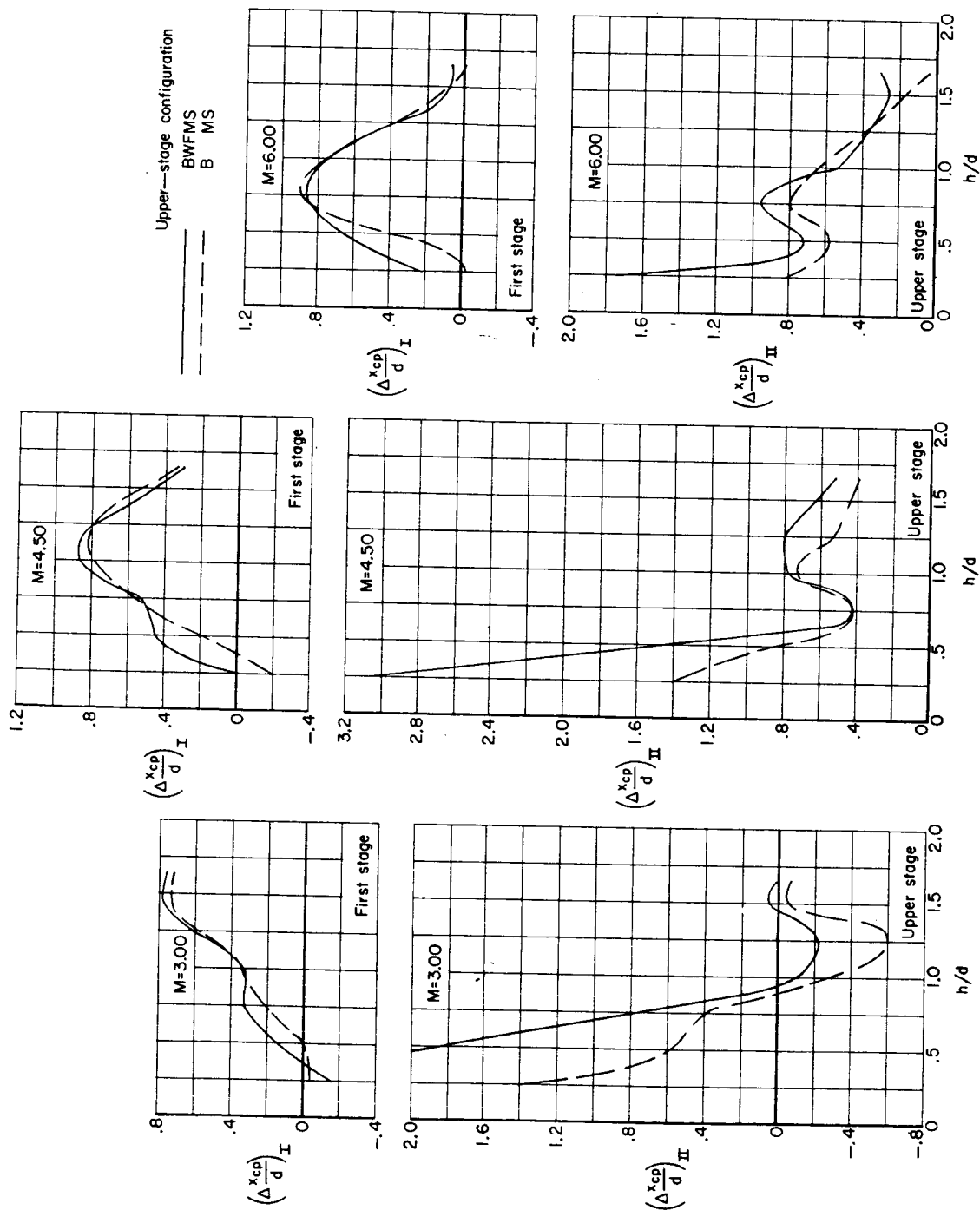
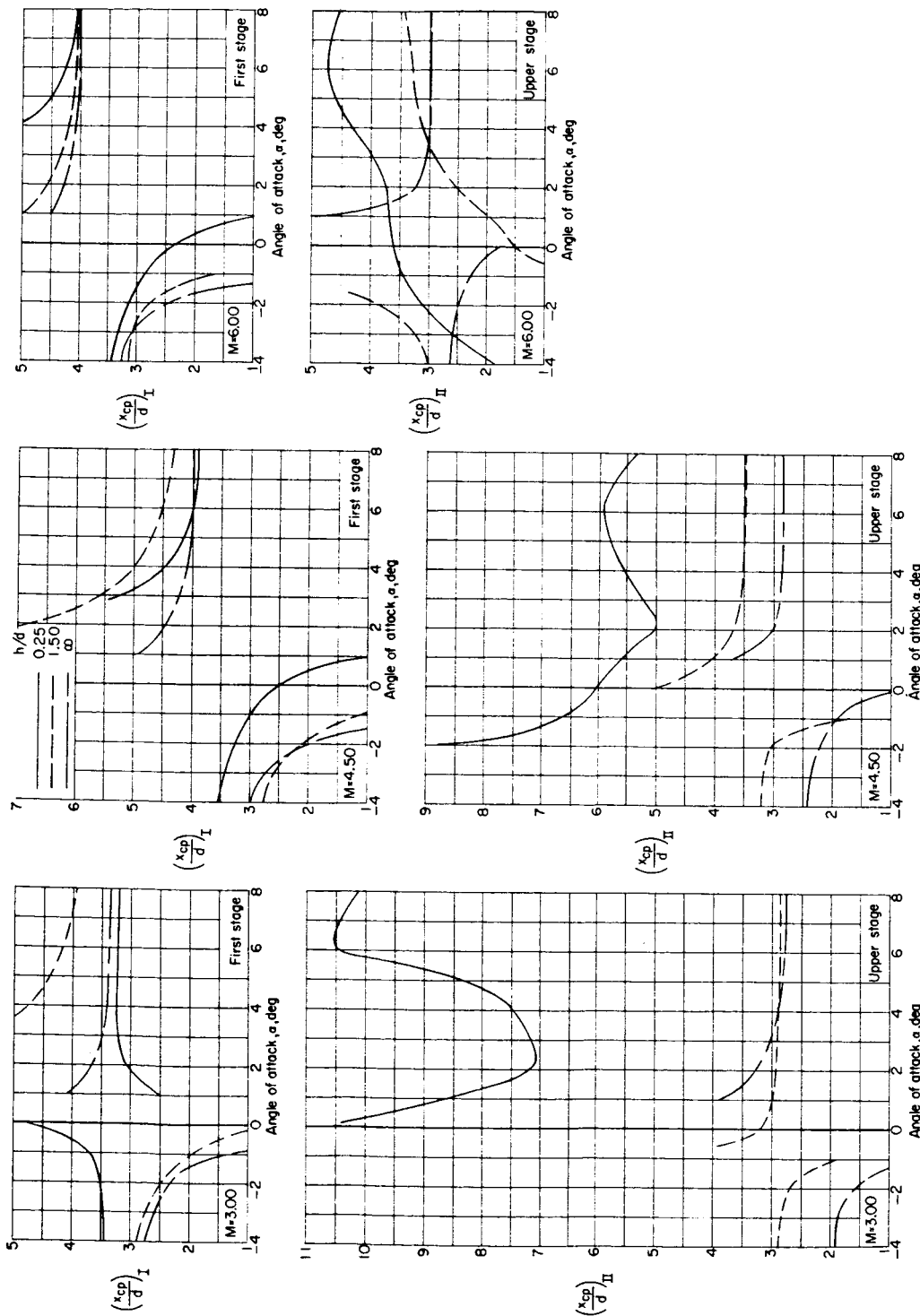


Figure 16.- Variation with spacing distance of the incremental changes in center of pressure at an angle of attack of 6° for the first-stage reusable booster in presence of various upper-stage configurations and for various upper-stage configurations in presence of the first-stage reusable booster.

~~CONFIDENTIAL~~

UNCLASSIFIED

UNCLASSIFIED  
CONFIDENTIAL



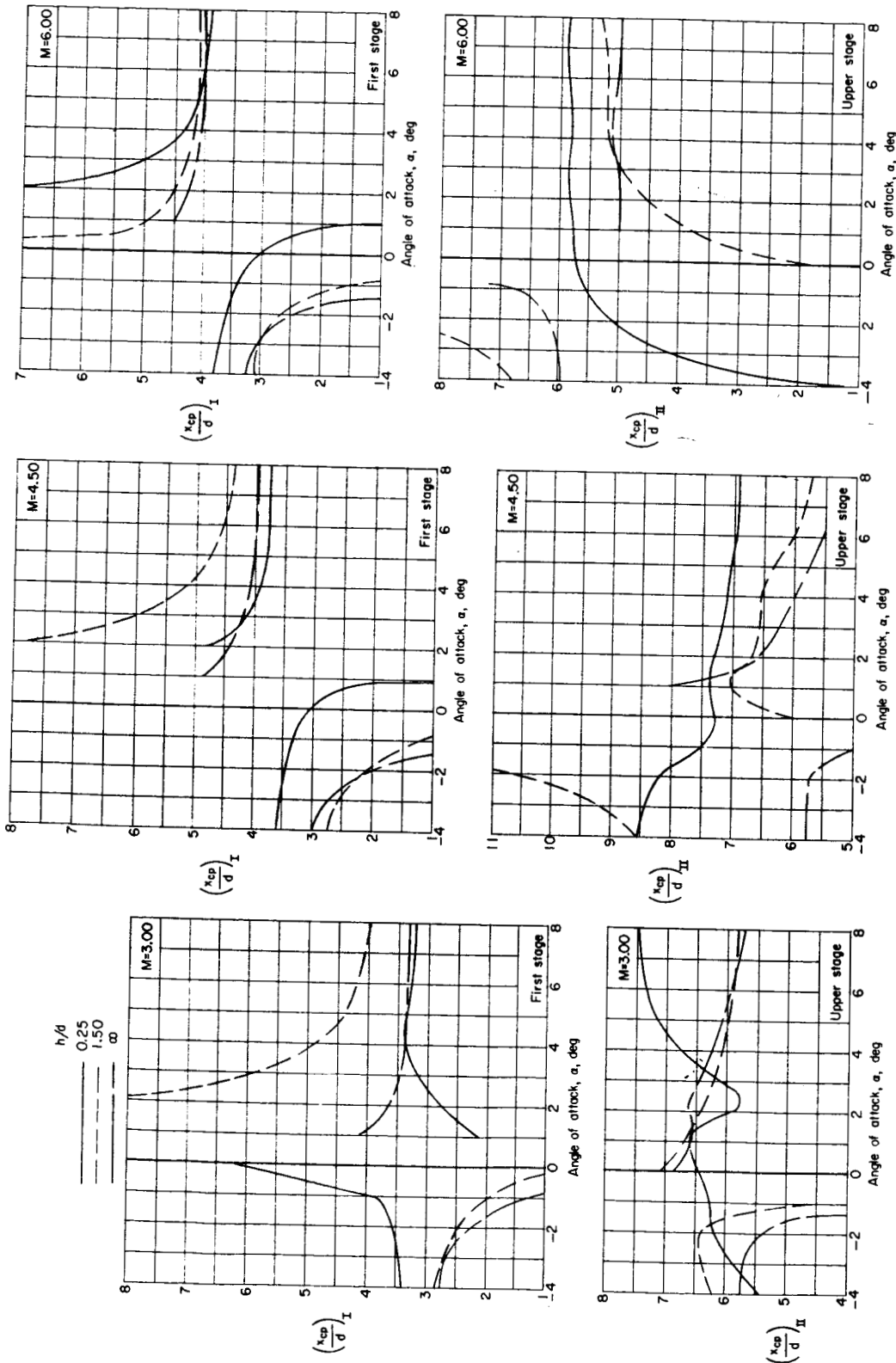
(a) Variation of center of pressure for the first stage in presence of BWFMS and for BWFMS in presence of the first stage.

Figure 17.- Variation of the center of pressure with angle of attack for the first-stage reusable booster in presence of various upper-stage configurations and for various upper-stage configurations in presence of the first-stage reusable booster.

CONFIDENTIAL

UNCLASSIFIED

UNCLASSIFIED  
~~CONFIDENTIAL~~



(b) Variation of center of pressure for the first stage in presence of BMS and for BMS in presence of the first stage.

Figure 17.- Concluded.